Physics – Uspekhi **68** (6) 597 – 616 (2025)

INSTRUMENTS AND METHODS OF INVESTIGATION PACS numbers: 68.65.Pq, 82.47.Uv, 88.80.fh

Graphene-based supercapacitors

A.V. Eletskii, K.L. Dao

DOI: https://doi.org/10.3367/UFNe.2024.11.039816

Contents

Abstract. Problems of supercapacitor development have been considered related to the enhancement of operating characteristics of systems such as specific energy storage, specific released energy, charging-discharging time, and the ability to withstand the maximum charge-discharge cycling times without lowering the stored energy. One of the approaches to solving the above-listed problems relates to the use of graphene and related materials as electrodes for supercapacitors. The presented article reviews studies addressing the investigation of graphene-based materials with the aim of their use in supercapacitors. Special attention is devoted to hybrid systems in which graphene-based materials are used in combination with metal oxides. Such systems, called pseudocapacitors, possess higher operation characteristics than conventional supercapacitors do due to the possibility of executing electro-chemical processes at the interface between the electrode and electrolyte.

Keywords: supercapacitors, pseudocapacitors, graphene

1. Introduction

The swift growth of world economies and a considerable enhancement of living standards lead to some worldwide problems, such as accelerated depletion of fossil fuel reserves and deterioration of the environmental situation (for example, increased greenhouse gas emissions and water and air pollution). For this reason, technologies with zero pollution and renewable energy sources are of paramount importance throughout the world.

In spite of some advances, problems related to energy storage and transportation remain topical. Contemporary energy storage methods possess some drawbacks which generate an urgent need to develop and create new systems fitting requirements of different energy problems.

Considerable attention of the scientific community has recently been focused on energy storage systems on the basis of supercapacitors (SCs). Keen interest in such devices is displayed by both academic and industry circles due to their distinct advantages over batteries and fuel elements, such as high specific power, short charge/discharge time, and long service life. The world market of SCs was estimated to be \$3.27 billion in 2019, and it will reach \$16.95 billion, according to expert predictions. This corresponds to an annual increase of 23.3% during the period 2020–2027 [1]. In the nearest future, SCs can become an alternative to the Li-ion accumulator due to a limited supply of Li as well as for safety reasons. In addition, SCs are more universal and stable than the conventional batteries which are widely used in mobile devices, portable media players, notebooks, etc.

Advantages of SCs over traditional energy storage and transportation devices are due to peculiarities in the principle of operation of these systems. The principle of operation of SCs of different kinds lies in accumulating energy in the double electric layer which is formed on the interface electrode/electrolyte. Operation indicators of SCs depend considerably on the characteristics of the electrode material and electrolyte. One of the best candidates for electrode material is graphene due to its unique characteristics, combining good electric conduction, a large specific surface, high chemical and thermal stability, high flexibility, and

A.V. Eletskii (*), **K.L. Dao** (**)
National Research University Moscow Power Engineering Institute, ul. Krasnokazarmennaya 14, 111250 Moscow, Russian Federation
E-mail: (*) eletskii@mail.ru, (**) linhdaokhanhsp2@gmail.com

Received 16 October 2024
Uspekhi Fizicheskikh Nauk **195** (6) 635 – 657 (2025)
Translated by A.V. Eletskii

perfect mechanical properties. At present, relatively simple and effective methods of large scale graphene production are being developed, which permits anticipating the industrial use of this material. Along with the methods developed on the early stage of graphene research, such as mechanical graphite exfoliation and chemical vapor deposition (CVD), considerably more productive approaches based on graphene oxide reduction have grown [2]. The approach based on chemical graphene oxide reduction is usually considered as an effective method of nonexpensive large-scale graphene production; however, this method requires the use of toxic, ecologically hazardous chemical compounds. The thermal graphene oxide reduction procedure does not have these disadvantages. While graphene flaxes obtained as a result of thermal graphene oxide reduction possess a considerable defect number, the high conductivity of this material offers the possibility to use it in supercapacitors.

The purpose of the present work is to investigate the possibility of designing SCs using graphene as an electrode material.

2. Supercapacitors: operation principle and advantages

The operation principle, operation characteristics, and specific models of SCs have been reviewed in detail by Yu.M. Volfkovich [3]. Supercapacitors (or ionistors, ultracapacitors) are relatively new electrochemical devices for the accumulation and storage of the electric energy and are similar to accumulators in construction and manufacturing. In their characteristics, SCs are in an intermediate position between conventional capacitors and accumulator batteries. Compared to batteries, SCs possess lower specific energy but a higher charge transport rate and higher energy density. Figure 1 shows a Ragon graph presenting values of the specific power and specific energy for typical energy storage and transformation devices [4, 5].

Table 1 compares advantages and disadvantages of SCs, traditional capacitors, and batteries in terms of their operation and cost characteristics.

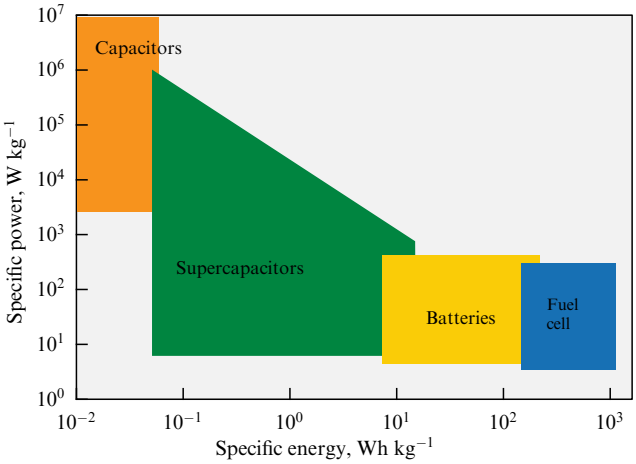

Figure 1. Comparative representation of specific power and specific energy for SC, conventional capacitors, batteries, and fuel elements [4].

Supercapacitors can be divided into 2 main groups: two-layer electrochemical supercapacitors and pseudocapacitors [8].

2.1 Two-layer electrochemical supercapacitors

In SCs of the first group, the electric energy is stored in the double electric layer as the energy of separation of ions of different signs. In this case, the charge accumulation mechanism is not Faraday, contains only physical charge transport, and does not involve redox reactions. For this reason, such SCs have a long life time. The surface charge appears as a result of different processes, including the surface dissociation of electrolyte ions and electrolyte ion adsorption in pores and on crystal defects of the electrode. Therewith, unlike charges are collected along the boundary electrode/electrolyte, while common electrical neutrality is retained. The double electrical layer thickness depends strongly on the electrolyte nature. It can change depending on the electrolyte concentration and the ion size. The energy storage of conventional capacitors is rather low due to the limited surface area covered with the

Table 1. Comparative characteristics of traditional capacitors, SCs, and batteries.

Characteristic	Traditional capacitors	Supercapacitors	Batteries	Literature
Specific power, W kg^{-1}	$< 100{,}000$	$< 10{,}000$	1000	[5]
Specific energy, Wh kg^{-1}	< 0.1	1–10	30–40	[5]
Charging time	$10^{-6}-10^{-3}$ s	0.3–30 s	1–5 h	[5]
Discharging time	$10^{-6}-10^{-3}$ s	0.3–30 s	0.3 – 3 h	[5]
Voltage	6–800 V	2.3–2.75 V/cell	1.2–4.2 V/cell	[5]
Life cycle	Close to infinity	$> 500{,}000$	~ 1000	[6]
Charge/discharge efficiency, %	95	85–98	70–85	[5]
Operation temperature, °C	−20 to +100	−40 to +85	−20 to +65	[5]
Cost, \$ kWh^{-1}	—	8000–10,000 (large system)	250–1000 (large system, Li-ion)	[7]
Cost, \$ kW^{-1}	—	8–12	100–200 (Li-ion)	[7]
Cost, \$ kg^{-1}	—	100 (large system)	100 (large system, Li-ion)	[6]

charge and geometry limitations on the distance between two charge plates. However, two-layer SCs can store considerably higher energy due to a larger inter-phase surface and the small distance between unlike charge layers.

The energy accumulation in two-layer SCs occurs as a result of the charge separation on the boundary between electrode and electrolyte. The energy E of an SC is expressed through the voltage U applied to its electrodes as follows:

$$E = \frac{1}{2} CU^2 , \tag{1}$$

where $C = \varepsilon\varepsilon_0 S/d$ is the capacity of the SC, ε is the dielectric constant, and ε_0 is the dielectric constant of the vacuum.

Electrochemical processes in a two-layer SC can be presented as [3, 9]
for the positive electrode:

$$E_{s1} + A^- \overset{\text{charging}}{\longrightarrow} E_{s1}^+//A^- + e^- ,$$
$$E_{s1}^+//A^- + e^- \overset{\text{discharging}}{\longrightarrow} E_{s1} + A^- ;$$

for the negative electrode:

$$E_{s2} + C^+ + e^- \overset{\text{charging}}{\longrightarrow} E_{s2}^-//C^+ ,$$
$$E_{s2}^-//C^+ \overset{\text{discharging}}{\longrightarrow} E_{s2} + C^+ + e^- ;$$

for the common charge/discharge process:

$$E_{s1} + E_{s2} + A^- + C^+ \overset{\text{charging}}{\longrightarrow} E_{s1}^+//A^- + E_{s2}^-//C^+ ,$$
$$E_{s1}^+//A^- + E_{s2}^-//C^+ \overset{\text{discharging}}{\longrightarrow} E_{s1} + E_{s2} + A^- + C^+ , \tag{2}$$

where E_{s1} and E_{s2} are the surface of the positive and negative electrode, correspondingly, // is the double electric layer, where the charges are located on both sides of the boundary, and A^- and C^+ are the anions and cations of the electrolyte, correspondingly.

In the charging process, electrons pass from the positive electrode to the negative one through the external power supply. Inside the electrolyte, cations move toward the negative electrode and anions move toward the positive electrode. During the discharge, electrons pass from the negative electrode to the positive one through the load. Therewith, the accumulated charge is released and the energy stored in the SC transforms into useful work. The ions adsorbed on the electrode surface return to the electrolyte. The electrode material is not practically experienced to structural and volumetric changes at such a mechanism of electrostatic charge accumulation and release. As a result, two-layer SCs can possess an extraordinarily long life charging/discharging cycle (usually from 10^5 to 10^6 cycles) [10]. Moreover, the charging/discharging process is easily reversible, because many kinetic processes, such as chemical reactions and diffusion, are not involved in it. The rate of charge accumulation and release can be very high, which results in quite high specific power of a two-layer SC (> 500 W kg^{-1}) [9, 10]. However, the main drawback of a two-layer SC is the much lower specific energy (< 10 Wh kg^{-1}) compared to batteries (35–150 Wh kg^{-1}). The reasons for this distinction are in the charge accumulation mechanism, which does not involve chemical processes, and in the limited charge accumulation region (boundary electrode/electrolyte) [10, 11].

2.2 Pseudocapacitors

Unlike the SCs of the first group, pseudocapacitors are based on Faraday redox reactions with the participation of metal oxide-based materials, metal-doped carbon, or conducting polymers. The electric capacity of pseudosupercapacitors depends on the chemical affinity of the electrode material to electrolyte ions. Pseudocapacitors possess a higher specific energy than two-layer SCs do. However, the drawback of such devices is determined by their operation principle, because the electrodes undergo mechanical stress during charge and discharge and degrade more rapidly. This gives rise to an increase in the inner resistance of SCs. Therefore, pseudocapacitors are characterized by a relatively low stability and cycling. Another essential drawback of pseudocapacitors is a rather slow charge/discharge rate.

Application of a potential to a pseudocapacitor results in a charge passing between the electrode and the electrolyte and in rapid and reversible redox reactions The charge/discharge mechanism in pseudocapacitors is similar to that for accumulators. The reaction on the positive electrode during charging can be represented as follows [12]:

$$E_1 + A^- \overset{\text{charging}}{\longrightarrow} E_1^{\delta+}//A^- + \delta e^- .$$

The reaction on the negative electrode is represented in the following manner:

$$E_2 + C^+ + \delta e^- \overset{\text{charging}}{\longrightarrow} E_2^{\delta-}//C^+ .$$

Here, E_1 and E_2 are the surfaces of the positive and negative electrode, respectively, // is the interface electrolyte/electrode, A^- and C^+ are the anions and cations of the electrolyte, respectively, and δe^- is the electrosorption valence related to the redox reactions.

Conway [13] identified several Faraday mechanisms which can promote an improvement in capacity characteristics: (1) underpotential deposition, (2) redox pseudocapacitance (as in $RuO_2 \cdot nH_2O$), and (3) intercalation pseudocapacitance. Figure 2 illustrates these mechanisms using the example of pseudocapacitors with Ru and Au electrodes.

Underpotential deposition occurs when metal ions form the adsorbed monolayer on the surface of another metal at a less negative potential than the equilibrium potential required for metal reduction. A classical example of the underpotential deposition is the deposition of lead on a gold electrode surface [14].

The *redox pseudocapacity* appears when ions are adsorbed electrochemically on the electrode surface or in its vicinity simultaneously with the Faraday charge transfer. Classical examples of pseudocapacity redox materials are metal oxides such as RuO_2, NiO, Co_3O_4, and MnO_2, as well as conducting polymers (polypirrol and polyanilin).

Intercalation pseudocapacitance relates to the intercalation of the charges generated as a result of a Faraday reaction between layers or in tunnels. This intercalation does not change the crystallography.

Besides the two types considered above, there are currently hybrid SCs, presenting a combination of two-layer SCs and pseudocapacitors. The main advantages of hybrid SCs relate to a higher volumetric and gravitational energy density and a possibility of providing higher currents. A higher energy density of hybrid SCs is caused by a Faraday reaction on the negative electrode. The positive electrode is usually fabricated from activated charcoal, so that the

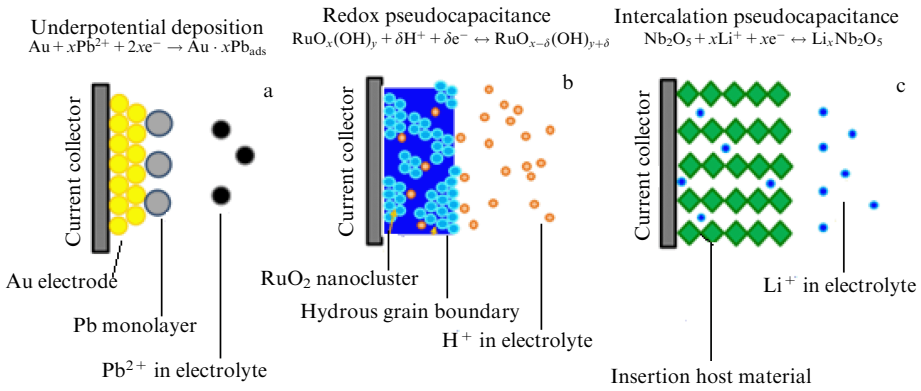

Figure 2. Abundant types of reversible Faraday mechanisms generating pseudocapacity: (a) deposition at reduced voltage; (b) redox pseudocapacity; and (c) intercalation pseudocapacity [12].

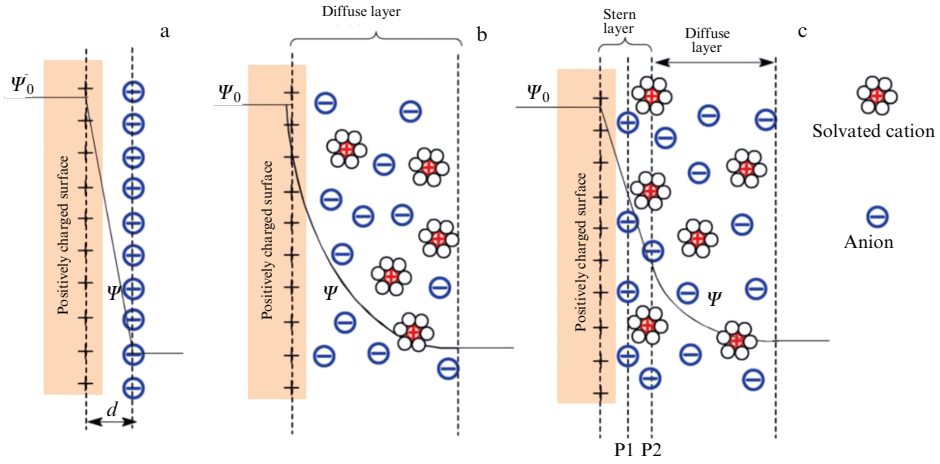

Figure 3. Models of double electric layer on positively charged surface: (a) Helmholtz model; (b) Gouy–Chapman model; (c) Stern model. P1 is internal Helmholtz surface; P2 is external Helmholtz surface; Ψ_0 and Ψ are potentials on electrode surface and on electrode/electrolyte interface, respectively [18].

electrostatic energy is accumulated in the double layer on the electrode surface. Due to the electrostatic interaction between charge carriers and the electrode surface (from the positive electrode side), hybrid SCs can provide quite high currents. Such devices are similar to Li-ion batteries in terms of construction and exploitation. At the moment, commercially accessible SCs are absent from the market, but they are under investigation in laboratory conditions [8].

One should note that the term 'supercapacitor' often means the classical two-layer SCs, which are the most studied and widely used devices.

2.3 Theory of double electric layer

The theory of the double electric layer was proposed by G.L.F. Helmholtz in 1853 [15] and was developed in detail by D.L. Chapman [16], O. Stern [17], and others. Figure 3 illustrates various models describing the structure of the double electric layer.

According to the Helmholtz theory, two layers of opposite sign form on the interface electrode/electrolyte. These layers are spaced from each other by the distance d, which is of the order of the atomic size (Fig. 3a). This model is relatively simple and is similar to the theory of conditional plane capacitors. The model was modified by Gouy and Chapman, who took into consideration the continuous distribution of electrolyte ions caused by thermal motion. They noted the existence of the diffusion layer (Fig. 3b). However, the Gouy–Chapman model overestimates the double electrical layer's capacity. The capacity of two separated charges is inversely proportional to the distance between them; therefore, in the case of ions with point charges placed close to the electrode surface, the model overestimates the capacity value. More recently, Stern combined the Helmholtz and Gouy models and developed a new model, according to which there are two regions of ion distribution: an internal region called a compact layer or Stern layer, and a diffusion layer (Fig. 3c). In the compact layer, ions are highly adsorbed by the electrode. There are the internal Helmholtz plane and the external Helmholtz plane spaced by the closest approach distance between specifically adsorbed ions (usually anions) and nonspecifically adsorbed ions of the opposite sign. The compact layer consists of specifically adsorbed ions (usually anions) and nonspecifically adsorbed ions of the opposite sign. The term 'specifically adsorbed ions' relates to the ions adsorbed on the electrode surface through the formation of chemical bonds or through the strong interaction usually associated with exchange or transfer of electrons. These ions normally make direct contact with the electrode surface and form the internal Helmholtz plane. Nonspecifically adsorbed ions of the opposite sign hold on the electrode surface by

weak physical forces such as electrostatic interaction without chemical bond formation. These ions are placed on the external Helmholtz plane and do not directly contact the electrode surface. The internal and the external Helmholtz planes are used to distinguish those two types of adsorbed ions. The closest approach distance between the specifically adsorbed ions (usually anions) and nonspecifically adsorbed ions of the opposite sign is of great importance. The external Helmholtz plane is also a boundary from which the diffusion layer begins. Therefore, the capacity of the double electric layer (C_{dl}) can be considered a combination of the capacity of the Stern compact double layer (C_H) and that of the diffusion region (C_{diff}), according to the following equation:

$$\frac{1}{C_{dl}} = \frac{1}{C_H} + \frac{1}{C_{diff}}. \quad (3)$$

The behavior of the double electric layer on a flat electrode surface depends on the electric field on the electrode, the solvent, in which electrolyte ions are dissolved, the types of electrolyte ions, and the chemical affinity between the adsorbed ions and the electrode surface. One should note also that the behavior of the double electric layer on the surface of pores of a porous electrode is more complicated than that on an infinite flat surface, since ion transport in a limited system is influenced by a set of factors such as the winding path of the mass transport, the limited space inside the pores, Ohmic resistance related to the electrolyte, and wetting the pore surface by the electrolyte.

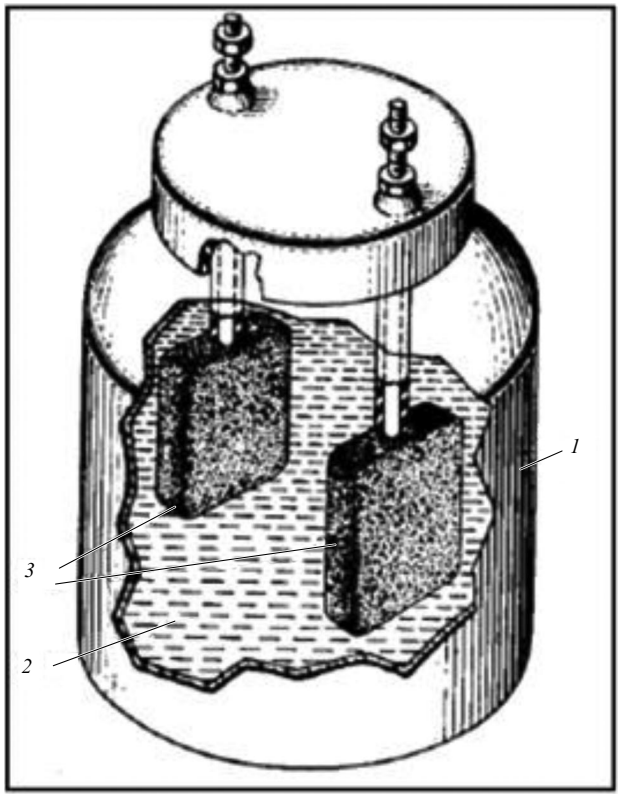

Figure 4. Becker's electrochemical capacitor [19]: (*1*) insulating layer, (*2*) acid electrolyte, (*3*) porous carbon electrodes.

2.4 History of invention and development of supercapacitors

While the first theory of the double electrical layer was elaborated even in 19th century, the history of the creation and development began only in the 1950s, almost 100 years later. The first experiments with capacitors with porous carbon electrodes were performed by an engineer group of the US company General Electric. In 1957, H.I. Becker [19] developed and patented the first electrochemical capacitor consisting of two electrodes immersed in a sulfur acid solution (Fig. 4). Such a configuration turned out to be impractical, and the Becker capacitor did not find a use. However, Becker's approach attracted a great deal of attention of other researchers and is considered as a starting point in the history of the elaboration of high capacitance electrochemical capacitors.

The standard configuration of SCs used now was invented by the chemist R.A. Rightmire from the Standard Oil Company (Ohio) in 1966. In 1971, Nippon Electronic Company, Japan, under license of the Standard Oil Company (Ohio), developed water-electrolyte capacitors for energy saving electronic systems This advance is considered to be the start of the commercial application of electrochemical capacitors or supercapacitors. Now, many companies, such as TESLA, Maxwell Technologies, Panasonic, Nesscap, EPCOS, NEC, ELNA, and TOKIN are investing heavily in the development and improvement of SCs [19–21].

Symmetric SCs, the most often found in practice, are presented schematically in Fig. 5. These devices consist, as a rule, of two electrodes with a developed surface separated by a porous membrane (separator) and immersed in an electrolyte.

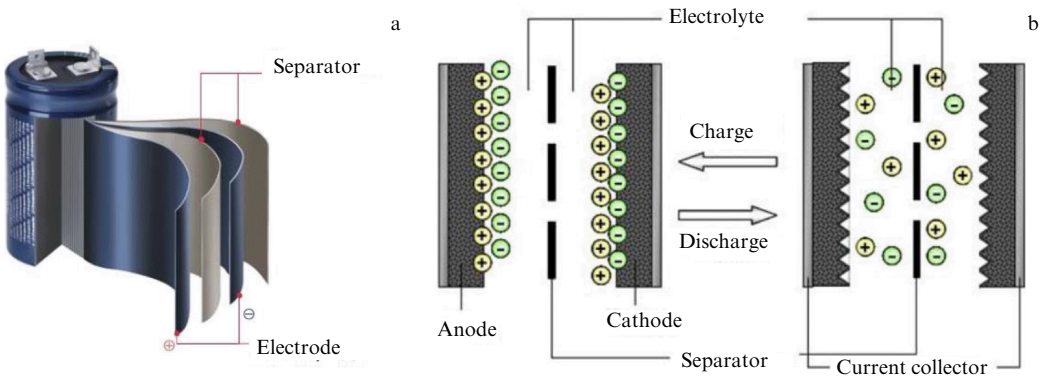

Figure 5. Structure of SC (a) and charge distribution in SC in charged and discharged states (b) [22].

The separator prevents the electric contact between oppositely charged electrodes.

As follows from Fig. 5, the SC operates on the basis of the reversible adsorption of oppositely charged ions on the electrode surface upon applying a potential, which results in the formation of the double electric layer on the electrode/electrolyte interface.

A large electric capacitance and, correspondingly, a higher stored energy of SCs than in traditional electric capacitors can be understood using simple estimations. The capacity C of a conventional capacitor, consisting of a dielectric (insulator) placed between two metal plates, is given by the formula [23]

$$C = \frac{Q}{V} = \varepsilon\varepsilon_0 \frac{S}{d}, \tag{4}$$

where Q is the electric charge; V is the electric potential; ε is the dielectric constant of the material separating the plates; ε_0 is the dielectric constant of the vacuum; S is the area of the metal plate; and d is the inter-plate distance.

On each interface electrode/electrolyte, a double electric layer is formed, so that the SC can be considered to be two capacitors connected in series (Fig. 5b). Therefore, the common capacity of the SC (C_{sc}) is determined as follows [4, 24, 25]:

$$\frac{1}{C_{sc}} = \frac{1}{C_1} + \frac{1}{C_2}, \tag{5}$$

where C_1 and C_2 are the capacities of two electrodes.

As already mentioned, the distance d between the charges in the double electric layer usually amounts to several nanometers ($\sim 10^{-9}$ m), while the specific surface area S of porous electrodes can reach values of 1000 $m^2\ g^{-1}$ or higher. The ratio S/d for SCs can reach values of the order of 10^{12} m g^{-1}. As a result, the specific electric capacity C_{sc} for SCs can reach values of 10–100 F g^{-1}. For comparison, the values S/d for conventional capacitors range within the interval $10-10^3$ m g^{-1}, and their specific capacities range within the interval $10^{-12}-10^{-6}$ F g^{-1}.

The energy of a capacitor E depends on its electric capacity C and is proportional to the square of the applied voltage U, according to the formula

$$E = \frac{1}{2} CU^2. \tag{6}$$

Formula (6) permits comparing the energy stored by a conventional capacitor and an SC. The voltage U for a conventional capacitor is severely limited by the electrostatic stability of the insulator and usually does not exceed 100 V. Therefore, its specific energy capacity ranges in the interval of 10^{-9}–10^{-2} J g^{-1}. The operation voltage of an SC depends mainly on the nature of the electrolyte. The lowest operation voltage is inherent in a water electrolyte SC and does not usually exceed 1.23 V (the voltage at which water electrolysis proceeds). Correspondingly, the specific energy capacity of such devices can reach values of 7–80 J g^{-1}. For an SC with nonwater electrolytes, this value can be higher by 3–4 times.

3. Electrolytes for supercapacitors

Conditions of supercapacitor operation depend to a large extent on the choice of the electrolyte. The development of optimal electrolytes for SCs has generated great interest around the world. Figure 6 presents the total number of published papers related to carbon SCs, electrolytes for SCs, hybrid SCs, and pseudocapacitors during the period from 2008 to 2018 and the distribution of these publications by country. As is seen, the contribution of Russian researchers to the development and elaboration of the field of SCs is rather negligible.

The electrolytes used in SCs can be divided into three groups: water, organic, and ion liquids. This classification is based on the nature of solutions. The first two types of electrolyte are prepared using water or organic solvents, while ion liquids do not contain solvents.

Besides of the above-listed electrolyte types, gel-polymer and redox-active electrolytes are also known. Solid or quasi-solid materials are also considered as prospective electrolytes for SCs [27, 28]. The classification of electrolytes for SCs is presented in Fig. 7.

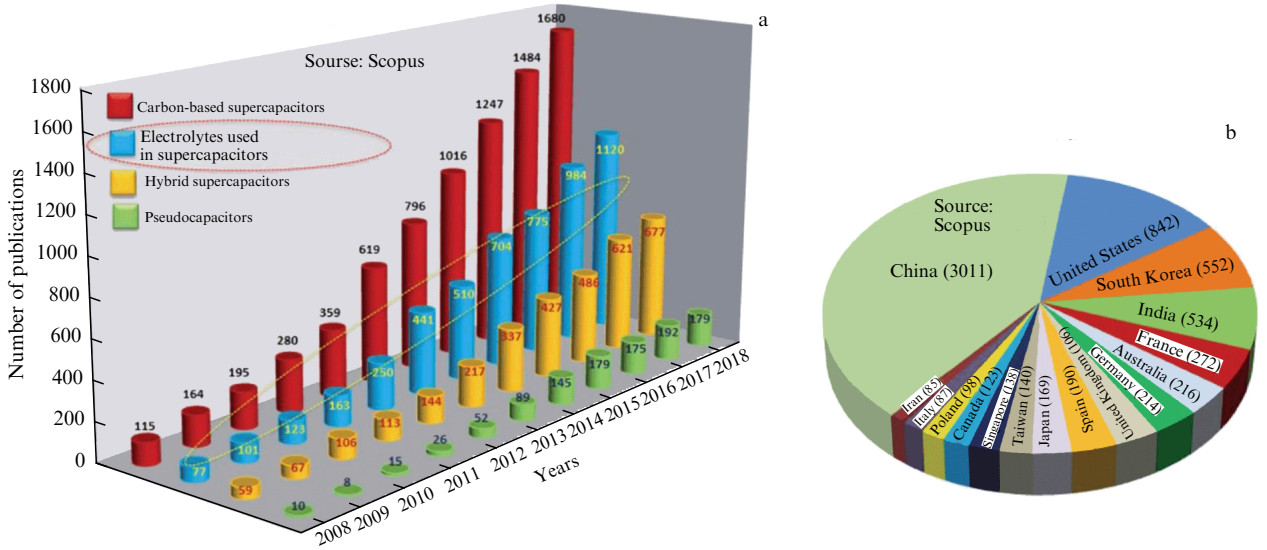

Figure 6. (a) Total number of publications related to carbon supercapacitors, electrolytes for SCs, hybrid SCs, and pseudocapacitors for period 2008–2018. (b) Distribution of publications related to electrolytes for SCs by country [26].

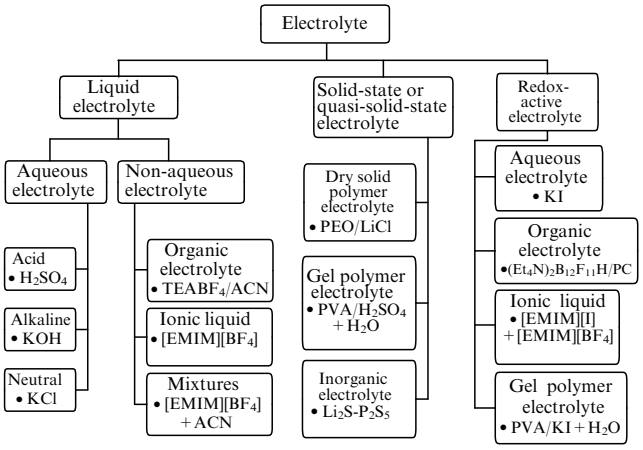

Figure 7. Classification of electrolytes for SCs [28, 29].

3.1 Water electrolyte

The family of water electrolytes can be divided into acid, alkali, and neutral solutions, the most useful components of which are H_2SO_4, KOH, and Na_2SO_4. The concentration of such solutions usually ranges between 0.5 and 6 M [29].

SCs based on water electrolytes possess quite high specific capacity due to the high dielectric constant of water (about 80) combined with the high polarizability of the H_2O molecule. Moreover, the water molecule is considerably smaller in size than organic solvent molecules. The high mobility of the ions H^+ and OH^- is due to their relatively small sizes and the mechanism of 'chain' transport. The chain transport of H^+ (protons) and OH^- (hydroxyl-ions) ions proceeds in water solutions where they pass from one water molecule to another through a series of intermediate steps. In the case of protons (H^+), this happens through the formation of hydroxonium ions H_3O^+ which transfer the proton to the next water molecule, forming a new H_3O^+ ion. A similar process also occurs in the case of OH^- ions, which promotes their high mobility and, as a consequence, a higher conductance of the water electrolyte and the current in the circuit of SCs based on water electrolytes than those based on nonwater electrolytes. In addition, water electrolytes can be prepared without strict control of the procedure and conditions. Their relatively low cost is also a great advantage.

A considerable drawback of water electrolytes limiting their application is the rather low value of the maximum allowable voltage (1.23 V), exceeding which results in the electrolysis of water. As was noted above, this parameter affects the values of the specific energy and power of SCs. The higher the voltage, the higher the values of these parameters. However, neutral electrolytes have been developed which allow a higher maximum voltage, reaching values of 2.0–2.3 V. A lesser corrosive effect and higher safety are also advantages of neutral electrolytes. This family of electrolytes includes salts of lithium (LiCl, Li_2SO_4, and $LiClO_4$), sodium (NaCl, Na_2SO_4, and $NaNO_3$), potassium (KCl, K_2SO_4, and KNO_3), calcium ($Ca(NO_3)_2$), and magnesium ($MgSO_4$) [29].

3.2 Organic electrolytes

As distinct from water electrolytes, organic electrolytes can operate at a voltage up to 3.5 V. This is a considerable advantage of organic electrolytes over water ones. Acetonitrile and propylene carbonate are usually used as solvents for organic electrolytes. Acetonitrile can dissolve a greater number of salts than other solvents can; however, it possesses toxicity and a harmful ecological effect. Electrolytes based on propylene carbonate are harmless and environmentally friendly. Moreover, they possess a wide range for changing the voltage, a wide operation temperature interval, and good conductance. Organic salts such as tetraethylammonium tetrafluoroborate, tetraethylphosfonium tetrafluoroborate, and threeethylmethylammonium tetrafluoroborate, are also used as electrolytes for SCs. As a rule, salts with a less symmetric structure possess a lower crystal-lattice energy and an enhanced solubility. However, it should be noted that organic electrolytes should not normally contain more than 3–5 ppm of water. Otherwise, the voltage of the SC will be reduced considerably [8].

In addition to the toxicity, a notable disadvantage of nonwater electrolytes relates to a rather low dielectric constant, which results in a lower value of the capacity of SCs than those with water electrolytes have. Furthermore, a higher viscosity of nonwater electrolytes results in a rather lower ion mobility and an enhanced internal resistance of the SC. There is often a loss in their operation capacity at low temperatures, for example, electrolytes based on propilene-carbonate [8, 29].

3.3 Ionic liquids

Ionic liquids are usually defined as salts consisting purely of ions and having a melting temperature lower than 100 °C [29]. Such liquids usually contain large organic cations and inorganic or organic anions. As distinct from classical nonwater electrolytes, ionic liquids posses a high thermostability (up to 300 °C) and a quite high value of the allowable voltage (up to 4.5 V) [30]. Disadvantages of ion liquids relate to their rather high cost, relatively low conductivity, and high viscosity, the last of which results in an enhancement of the internal resistance of the SC, resulting in a lower specific power. Such disadvantages considerably limit the industrial usage of ionic liquid-based SCs. A small group of proton ionic liquids are known to contain formate, nitrate, or lactate. These liquids have a quite high dielectric constant. However, the possibility of their usage as electrolytes in SCs has not yet been studied, which is probably explained by their high cost and the low electrochemical stability of anions in organic nonfluorinated acids [29].

4. Electrode materials for supercapacitors

Another important issue in the design of SCs relates to the choice of electrode material. The electrode material structure affects not only the electric capacity but also the energy density and power of the device. Electrode materials for SCs can be divided onto three main groups: materials for two-layer SCs, materials with pseudocapacity, and conducting polymers incorporated into electrode materials.

4.1 Materials for two-layer supercapacitors

Various carbon modifications are usually used as materials with a two-layer capacity [19]. This group of modifications includes carbon nanotubes, graphene, graphene oxide, and nanostructured graphite. Such structures are characterized by a high specific surface area, accessibility, and well-developed production technologies. The energy storage mechanism with the usage of carbon materials is based on the formation of a double electric layer on the electrode/electrolyte interface, so that the electrode capacity depends mainly on the area of the

Table 2. Characteristics of carbon-based materials for supercapacitors.

Carbon material	Specific surface area, $m^2\ g^{-1}$	Specific capacity, $F\ g^{-1}$	Literature
Activated carbon	~ 2000	94–413	[31]
Activated carbon fiber	~ 1200	60–300	[31]
Carbon aerogel	400–1000	100–125	[32, 33]
Carbon nanotubes	120–1035	15–135	[32, 33]
Graphene-based materials	< 1500	14–264	[33]

surface accessible for electrolyte ions. Important factors affecting the electrochemical characteristics of carbon-based SCs are the specific surface area, form, and structure of pores, the size distribution of the pores, the functionality of the surface, and the electric conductance. A high specific surface area of carbon nanomaterials determines their high capacity to accumulate a charge at the electrode/electrolyte interface.

Table 2 presents characteristics of some carbon materials often used as electrodes for SCs.

Each carbon material has its advantages and disadvantages. A gain in the functional properties of a material can be accompanied by difficulty producing it and therefore its high cost. A prominent example of such material is carbon nanotubes. Their use promotes a considerable enhancement of the energy density of SCs due to their unique tubular structure and high electric characteristics. However, an essential drawback of carbon nanotubes relates to their rather high production cost, considerably limiting their industrial use. Another example is graphene, having a two-dimensional carbon nanostructure. With a high specific surface area and high conductivity, it wrinkles easily, which presents difficulties in fabricating an electrode. 3D materials such as activated graphite and a patterned carbon material are promising due to a high specific surface area and the existence of numerous developed pores. However, the specific capacity value of such material is lower than that for carbon nanotubes and graphene due to a high number of pores and a rather low conductivity [34, 35].

One should note that the contemporary production of commercial SCs uses mainly activated graphite as the electrode material. Its production procedure includes various physical, chemical, and activation stages.

According to the IUPAC classification, carbon materials are divided depending on the pore size into microporous (< 2 nm), mesoporous (from 2 to 50 nm), and macroporous (> 50 nm) [36].

If the pore size of a carbon material is too small, the diffusion of solvated ions in the pores is hindered, which in turn results in a decrease in the effective inner surface area for double electric layer formation. This is especially pronounced in the case of relatively large ion size. Conversely, large pores are easily accessible for ions; however, in this case, the common pore surface area is considerable lower. Therefore, the most proper carbon-based materials for SCs are mesoporous rather than microporous or macroporous structures.

4.2 Pseudocapacitance materials

Oxides are the most widely studied pseudocapacitance materials. Metal oxides provide a higher energy density for SCs than conventional carbon-based materials do, because a considerable contribution to SC capacitance relates to the redox reaction of metal oxides.

The most studied metal oxide used for SC electrodes is RuO_2. The specific capacity of an SC with sulfur acid as electrolyte amounts to about 750 $F\ g^{-1}$. Note that the contribution of the double electric layer to the capacity of such an SC amounts to about 10% [8]. Other promising materials for SC electrodes are transition metal oxides: NiO, MnO_2, Co_2O_3, Co_3O_4, V_2O_5, etc. [8]. However, the problem of forming a surface with high activity using such metal oxides has not yet been resolved. Moreover, the possibility of wide usage of metal oxides as SC electrodes is limited by their rather high cost.

4.3 Conducting polymers incorporated into electrode materials

Conducting polymer is one more class of materials used in SCs. Its advantages relate to a comparatively low cost, a simple synthesis procedure, stability against oxidation in air, and a higher electric conductance than transition metal oxides employed in electrodes. Such conducting polymers as polyaniline, polypyrrole, and polythiophene should be mentioned first. SCs with the use of polyaniline (PANI) incorporated into the electrode structure demonstrate a quite high specific capacity between 233 and 1220 $F\ g^{-1}$ [8].

A considerable disadvantage of conducting polymer relates to its instability in charging/discharging processes. This is caused by the mechanical degradation of the electrode and deterioration of electrochemical characteristics as a result of cycling. For example, the specific capacity of polypyrrole-based electrodes can decrease by 50% after 1000 charging/discharging cycles [8].

Note that at the present time studies on composite electrode materials are actively being performed. For example, the specific capacity value for PANI composites with graphene oxide ranges between 210 and 1130 $F\ g^{-1}$. Great attention is paid to investigations on the properties of the hybrid structure of manganese oxide with various carbon materials (activated graphite, carbon aerogels, carbon nanotubes, graphene, etc.) [8].

5. Graphene as electrode material

Graphene, first obtained in 2004 [128] and presenting an allotrope carbon modification, attracts fast-growing attention. Due to its unique structure, graphene possesses some remarkable properties, such as a high specific surface area, high electric conductivity, high chemical and thermal stability, high flexibility, and superior mechanical characteristics. These unique properties make graphene a good material for energy storage in SCs.

5.1 Structure of graphene

Graphene has the form of a flat 2D hexagonal structure one atom thick, in which carbon atoms interact with each other through sp^2 bonds. Three out of four electrons belonging to the external shell of a carbon atom occupy three hybrid sp^2 orbitals s, p_x, and p_y, forming σ-bonds and providing the graphene stability. As is shown in Fig. 8, these bonds have a length of about 0.142 nm. The rest of the electron occupies the p_z orbital, forming the π-bond which is oriented perpendicular to the lattice plane and is responsible for conduction in graphene and other electronic properties [37].

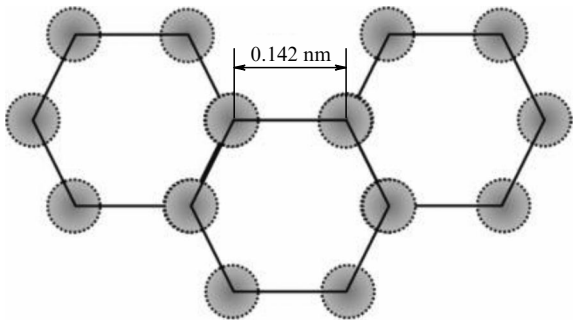

Figure 8. Hexagonal graphene structure [37].

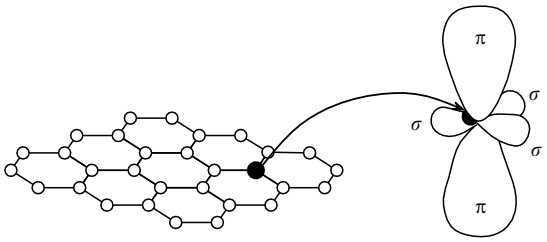

Figure 9. Bonds of each carbon atom in graphene lattice [38].

Figure 9 presents the bonds of each carbon atom in the graphene lattice.

Graphene can be considered an initial structure of other carbon materials, including rolled-up 0D fullerenes, rolled-up 1D nanotubes, and 3D graphite, as is shown in Fig. 10 [39, 40].

The thickness of a graphene layer is estimated as 0.35 nm, which is about 1/200,000 the diameter of a human hair. Nevertheless, the structure of graphene is quite stable. Carbon atoms are bound quite strongly to each other, withstanding external stress. Electron properties of a graphene sheet considerably depend on the boundary structure. Three boundary types are distinguished: armchair, zigzag, and an arbitrary orientation angle of the boundary relating to the graphene sheet axis (Fig. 11). The variety of boundary structures results in different conduction characteristics. Graphene nanoribbon with a zigzag boundary usually behaves like a metal, while a nanoribbon with the armchair boundary conducts electricity like a metal or a superconductor, depending on its width [37].

5.2 Properties of graphene

Among the various candidates for SC electrode material, graphene has attracted growing attention due to its extraordinary properties. The three following factors indicate its high potential as electrode material for supercapacitors of the new generation:

• Graphene possesses the highest known specific surface area, 2630 $m^2\ g^{-1}$ [41], and a quite low theoretical density of 2.28 g cm^{-3} [42]. Due to these characteristics, the material combines a high capacity to close packaging and a very high specific surface area for the interaction of electrons and ions.

• Graphene possesses superior electric conduction and very high electron mobility reaching 200,000 $cm^2\ V^{-1}\ s^{-1}$ at room temperature [40, 43, 44], which provides fast electron and ion transport through various interfaces (electrode/electrolyte and electrode/current collector). In addition, due to its high electric conductivity, graphene can act simultaneously as an active material and a current collector. This permits avoiding the use of additional materials such as binders and dopants.

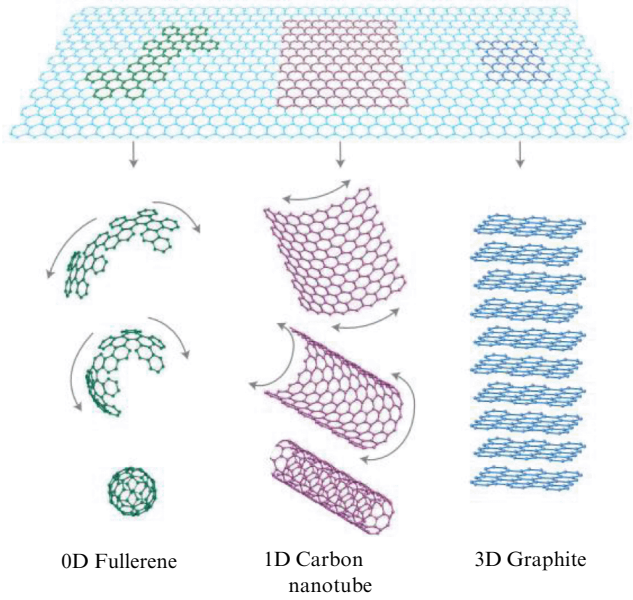

Figure 10. Graphene is a 2D structural material for carbon nanomaterials of other dimensions [39].

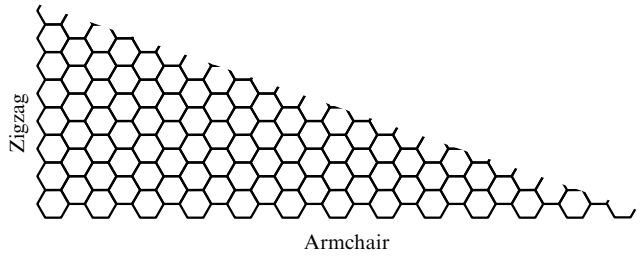

Figure 11. Types of boundaries of a graphene nanoribbon [37].

• Graphene also demonstrates a high mechanical strength, with a Young modulus of ~ 1 TPa and reversible deformation up to 25% [45] upon saving a high specific capacity. This makes it suitable for use in flexible electronics and printing electronics.

Graphene consists of only one carbon atomic layer; therefore, it is superthin and superlight, which is an advantage. Its planar density amounts to 0.77 mg nm^{-2}. As is shown in Fig. 8, the elementary graphene structure constitutes a hexagonal carbon ring of 0.052 nm^2 in area. In such a structure, each carbon atom belongs to three rings. Due to its one-atom thickness, graphene possesses very high transparency — 97.7%, i.e., it absorbs only 2.3% of visible light [46].

5.3 Methods of graphene production

Various methods have been used for graphene production (see, for example, review [129]), such as mechanical exfoliation of graphite (widely known as the scotch method) [40] and chemical vapor deposition (CVD) [47, 48]. However, both these methods are characterized by rather low productivity and high production costs and are hardly proper for large-scale graphene production. A possibility of producing a large

graphene mass is provided by the usage of oxide graphene reduction. The most useful methods of graphene reduction are chemical and thermal reduction due to a relatively easy realization and the quality of the final product. The chemical graphene oxide reduction method requires the use of toxic and environmentally harmful reagents. For this reason, the most preferable method of graphene oxide reduction is thermal reduction, which is characterized by a relatively simple procedure and does not requires the use of poisonous reagents [49, 50].

Graphene and graphene oxide are different in their structure. The difference relates mainly to a large number of functional oxygen groups, including epoxy (C–O–C), single-bond oxygen (C–O), hydroxyl (C–OH), and carbonyl (C=O) groups [41, 51] attached to carbon plates and structural defects of these planes. Graphene oxide barely conducts electricity. Graphene oxide reduction results in a partial reduction of the structure and properties of graphene as well as partial removal of structural defects. Properties of reduced graphene oxide depend on the parameters of the reduction procedure. The thermal processing temperature plays an important role in the procedure, because it determines the quality of the final product. Increasing the thermal processing temperature too fast promotes explosion-like damage to the material, so the heating rate should be limited to a value of the order of 1 K min^{-1} [52].

A sudden temperature jump causes a thermal shock, and functional groups H_2O, CO, and CO_2 are removed from the graphene oxide lattice. The release of gases creates pressure between neighboring graphene oxide layers, which is a reason for the exfoliation. According to the equation of state, a pressure of 40 MPa is reached at 300 °C, while at 1000 °C the pressure increases to 130 MPa [53], while an estimation of the Gamaker constant indicates that only 2.5 MPa is sufficient for the exfoliation of a graphene layer [53]. In the temperature range between 140 and 180 °C, evaporation of intercalated water molecules dominates, while the main carboxyl groups are removed at a further temperature growth between 180 and 600 °C. Removal of all the remaining carbonyl and part of the hydroxyl groups occurs in the temperature range of 600–800 °C. A further temperature increase to about 1000 °C results in removal of the remaining hydroxyl and part of the epoxy groups, leading to the formation of a large quantity of structural defects caused by plane C=C cracking [54]. It was reported in [55] that the ratio C/O amounts to less than 7 for a processing temperature of less than 500 °C, and as the temperature reaches 750 °C, this ratio exceeds 13.

Both the annealing temperature and annealing atmosphere are important for thermal graphene oxide reduction. Because the oxidation rate grows sharply with the temperature, gaseous oxygen should be excluded during annealing. For this reason, thermal reduction is usually carried out in a vacuum [56], in an inert media [57], or in a reductive gas atmosphere [57–60]. Experiments [57] indicate that the key factor providing reduction of graphene oxide is a strong vacuum ($< 10^{-5}$ Torr), because otherwise the films are destroyed easily as a result of the reaction with the rest of the oxygen. This condition should be taken into account in the case of an inert atmosphere. For this reason, a reduction gas such as H_2 is added to bind the rest of the oxygen. What is more, the oxide graphene reduction in an H_2 atmosphere can be performed at a relatively low temperature due to the high reduction capacity of hydrogen. Graphene oxide reduces well in 2 h at 450 °C in the mixture Ar/H_2 (1:1), which results in a C/O ratio of 14.9 and electric conductivity of about 10^3 S cm^{-1} [49]. Removal of oxygen-containing groups during graphene oxide reduction causes an enhancement of the electric conductivity. An abrupt jump in the conductivity occurs within the temperature range of 150–200 °C, where conductivity changes by five orders of magnitude, from 10^{-3} up to 100 S m^{-1}. The maximum conductivity (about 3500 S m^{-1}) reached at a temperature of 800 °C is about an order of magnitude lower than the reference value of the conductivity of graphite. However, heating samples results in a decrease in their density by 2.4 times (from 1.2 down to 0.5 g cm^{-3}). Taking into account that the density of reduced graphene oxide processed at 800 °C amounts to about 0.5 g cm^{-3}, which is less than that of crystalline graphite (2.2 g cm^{-3}), we find that the conductivity of the reduced graphene oxide calculated for one layer is one half that of graphite [61].

The main drawback of the method of graphene production based on the thermal reduction of oxide graphene is related to graphene layers being damaged due to an increase in gas pressure and carbon dioxide emission because of heating. Besides the damage to the graphene structure, this causes about a 30% decrease in the oxide graphene mass, which generates defects and vacancies. The mechanical strength of the graphene produced can also be affected [62].

5.4 Graphene as electrode material

Using graphene as the electrode of an SC was demonstrated in the innovative work of Stoller et al. [41]. Chemically modified graphene (CMG) produced by mechanical exfoliation of graphite was utilized as the electrode material. Its specific capacity amounted to 135 F g^{-1} and 99 F g^{-1} in water and organic electrolytes, respectively. Figure 12a presents a SEM image of agglomerate particle surfaces. Figure 12b, obtained by means of a transmission electron microscope (TEM), shows individual graphene sheets protruding from the outer surface. TEM images of the surface of the prepared electrode with low and high amplification are presented in Fig. 12c. An illustration of a two-electrode testing cell of an SC is shown in Fig. 12d.

Recent attention has been focused on the possibility of developing and using many graphene-based structures. Studies consider graphene-based electrode materials according to their macrostructural complexity, i.e., 0D (free-standing graphene dots and particles), 1D (fibrous and thread-like structures), 2D (graphene and graphene-based films, and 3D (graphene foams and composites) [63]. A short description of these structures and consideration of the potential to use them as elements of SCs are presented below.

5.4.1 Graphene dots and powders as electrodes of SCs. Graphene dots and particles can be produced as a result of oxidation and exfoliation of graphite followed by the controlled reduction of graphene oxide (by means of a reduction reagent such as hydrazine-hydrate). Graphene particles produced are prone to agglomeration, and reduced graphene oxide becomes hydrophobic, which affects further treatment in water or water solutions. On the contrary, graphene oxide is a unique amphiphile with negatively charged hydrophilic edges and a hydrophobic basal plane. This unique feature offers the possibility of selective interaction of graphene oxide with some surface-active substances (SASs), thereby providing control of the graphene oxide amphiphility.

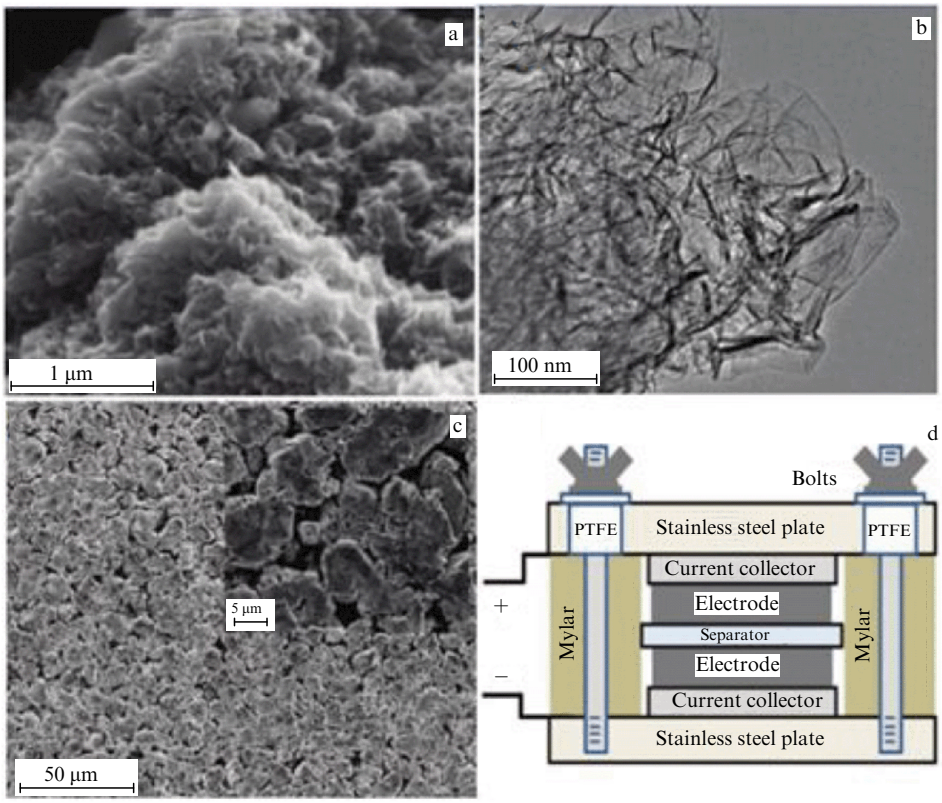

Figure 12. (a) SEM images of CMG particle surfaces, (b) TEM images showing individual graphene sheets protruding from surface of CMG particles, (c) TEM images of electrode surface with low and high (inset) amplification, (d) cell assembly [41].

Zhang et al. [64] studied graphene-based materials stabilized by SASs such as tetrabutilammonium hydroxide (TBAOH), cethyltrimethylammonium bromide (CTAB), and sodium dodecylbenzenesulphonate [64, 65]. They found that reduced graphene oxide sheets can be intercalated by SASs. A supercapacitor with the graphene stabilized by a TBAOH electrode possesses a specific capacity of 194 F g^{-1} at the specific current of 1 A g^{-1}, which is caused in part by a decrease in the orientation degree of reduced graphene oxide and enhancement of wettability in the presence of an intercalated SAS. In addition, the SAS modification permits one to disperse homogeneously reduced graphene oxide in water solutions. Table 3 presents results of testing graphene-based SC stabilized by SASs.

SC electrodes fabricated from graphene powders usually demonstrate a high specific power due to a large specific surface area and good conductivity. However, they possess a rather low specific capacity (about 200 F g^{-1}). Therefore, the specific energy and the overall productivity of the device are limited, as a rule. On the contrary, the usage of some transition metal oxides (MnO_2, RuO_2, NiO, Co_3O_4, and Fe_3O_4) or hydroxides ($Ni(OH)_2$ and $Co(OH)_2$), as well as conducting polymers (PANI, polypyrroles, and polythiophenes) provide a higher specific capacity as a result of reversible Faraday redox reactions on the electrode surface. Graphene-based materials represent a key electrode material for a two-layer capacity. An effective combination of the two-layer capacity and the pseudocapacity can be made by means of the development of hybrid electrodes through the integration of metal oxides/hydroxides of conducting polymers with a graphite grid. In hybrid electrodes, graphene is used as a conducting channel for the charge transport, which improves the overall conduction, while the pseudocapacity appears from metal oxides/hydroxides or conducting polymers.

One graphene-oxide metal composite, graphene/MnO_2 composite, has been studied in detail. A simple approach to the production of graphene/MnO_2 hydrothermally reduced composites has been developed by Yang et al. [66]. Their measurements indicate that the specific capacity of a composite powder amounts to 211.5 F g^{-1} at the potential scanning rate of 2 mV s^{-1}. Therewith, about 75% of the capacity remains after 1000 charging/discharging cycles in

Table 3. Characteristics of graphene-based SCs stabilized by SASs.

Electrode material	SAS	Electrolyte	Testing conditions	Capacity, F g^{-1}	Literature
Graphene stabilized by SASs	TBAOH	2M H_2SO_4	1 A g^{-1}	194	[64]
	CTAB			116	
	SDBS			159	
Graphene/polyaniline stabilized by SASs	TBAOH	2M H_2SO_4	0.2 A g^{-1}	526	[65]
	SDBS			480	

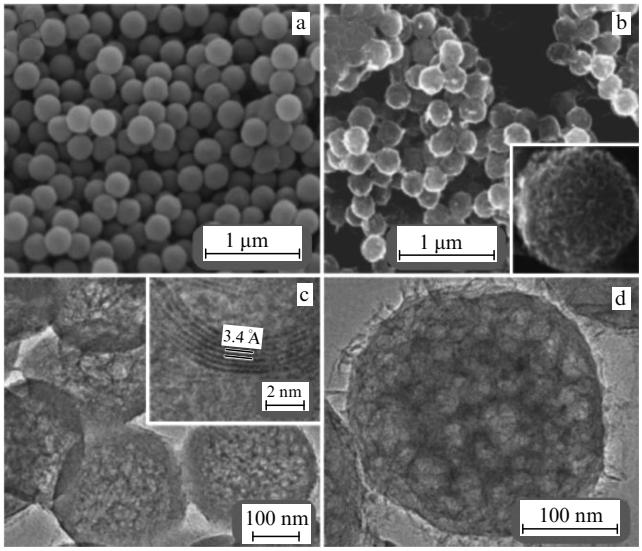

Figure 13. SEM images of SPS-COOH: (a) mesoporous graphene nanoballs; (b) nanoballs produced for sample (a) of mesoporous graphene nanoballs; (b) balls produced by CVD method from the sample (a); (c) TEM images of mesoporous graphene nanoballs in vicinity of edges; (d) amplified image of individual graphene ball with nanopores [70].

1 M Na_2SO_4 electrolyte. Dai et al. [67] synthesized nanoplates $Ni(OH)_2$ on graphene sheets. The hybrid electrode material possesses a high specific power and energy and a high specific capacity of about 1335 F g^{-1} at a specific charging/discharging current of 2.8 A g^{-1} and about 953 F g^{-1} at 45.7 A g^{-1}. These graphene-based metal oxides/hydroxides were prepared through the reduction of graphene oxide followed by loading pseudocapacitive materials. However, agglomeration of graphene particles and a rather low content of micropores necessary for electrochemical energy storage prevent complete usage of the superior electric and surface properties of graphene [68].

Several processes have been developed using templates to enhance the conductivity and the specific surface area of composites. Yoon et al. [69] developed a method to synthesize hollow graphene balls using Ni nanoparticles as a template. This method involves the carbonization process for facilitating the transfer of carbon into Ni nanoparticles by means of a polyol solution. Thereafter, the material underwent thermal annealing, stimulating the segregation of carbon, which resulted in the formation of a graphene layer on the surface of Ni nanoparticles. The graphene balls produced preserve their spherical structure and dispersion during the thermal annealing process even after removing the main Ni nanoparticle template. Mesoporous graphene nanoballs (MGBs) were mass produced by Lee et al. [70] in a similar manner by means of the CVD method using a precursor. Figure 13 presents the morphology of polymer spheres and mesoporous graphene nanoballs produced by the CVD method with the use of a precursor. Figure 13a shows SPS-COOH spheres about 250 nm in diameter, which are practically homogeneous in size and morphology. An enhanced SEM image of an individual mesoporous graphene ball is given in the inset to Fig. 13b. Mesoporous graphene nanoballs 4.27 nm in pore diameter and 508 m^2 g^{-1} in specific surface area are presented in Fig. 13c, d. As is seen in the inset to Fig. 13c, a mesoporous graphene nanoball contains about 7 layers with an inter-layer distance of 0.34 nm. Supercapacitors with mesoporous graphene nanoball electrodes demonstrate a specific capacity of 206 F g^{-1}, more than 96% of which remains after 10,000 cycles.

Very recently, Park et al. [71] produced micro/macro-sized powder from graphene nanosheets. To prepare microspheres, they used the self-assembly process by spraying with the use of a high temperature organic solvent. The SC electrode produced demonstrates a specific capacity of 151 F g^{-1} at a scanning rate of 10 mV s^{-1}.

Results of studies of SCs based on graphene dots and powders are presented in Table 4, containing the production method and capacity values.

5.4.2 1D graphene-based electrode materials (1D fibers and threads based on graphene). Graphene-based fibers and threads have a great application potential due to a combination of such advantages as small size, high flexibility, and braiding ability, which promises some applications in SCs of the next generation used in portable devices and electric transport facilities. Carbon-based materials such as carbon fibers, carbon nanotubes (CNTs), graphene, and mesoporous carbon can be transformed into filaments of various struc-

Table 4. Characteristics of various SCs based on graphene dots and powders.

Electrode material	Method	Electrolyte	Testing conditions	Specific capacity, F g^{-1}	Specific surface area, m^2 g^{-1}	Literature
Hydrothermally reduced graphene/MnO_2	Redox deposition	1M Na_2SO_4	2 mV s^{-1}	211.5	—	[66]
$Ni(OH)_2$/graphene sheets	Hydrothermal	3M NaCl	2.8 A g^{-1}	1335	—	[67]
			45.7 A g^{-1}	953	—	
Reduced graphene oxide/Co_3O_4	Chemical deposition	6M KOH	1 A g^{-1}	291	—	[68]
Mesoporous graphene nanoballs	Chemical vapor deposition	1M H_2SO_4	5 mV s^{-1}	206	508	[70]
Graphene microsphere	Spray-assisted deep-frying process	1M H_2SO_4	10 mV s^{-1}	151	365	[71]
Fe_3O_4/reduced graphene oxide	Hydrothermal	1M KOH	1 A g^{-1}	169	127.7	[72]
Reduced graphene oxide/Pluronic F127	Hydrothermal, thermal annealing	6M KOH	1 mV s^{-1}	210	696	[73]

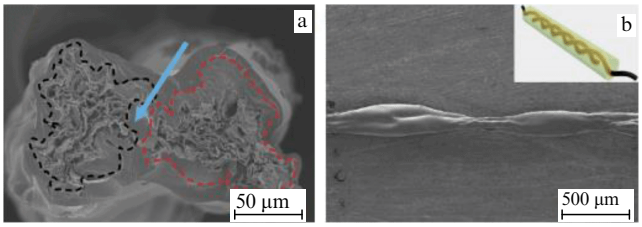

Figure 14. SEM images of cross section (a) and side view (b) of an SC based on coaxial filaments [75].

tures. They can also be joined to selected electroactive materials possessing Faraday pseudocapacity, such as metal oxides, hydroxides, and conducting polymers (for example, polypyrrole, polyaniline (PANI), poly3,4-ethylendioxythiophene (PEDOT)).

A solid electrochemical capacitor fabricated from filaments of reduced graphene oxide covered by gold wires demonstrates a quite high specific capacity of 6.49 mF cm^{-2}, which decreases by less than 1%, even upon bending by 120° or twisting into an S-like structure. Meng et al. [74] developed a fully graphene SC for the purpose of lowering the electrode material mass. In this device, gold wires serving as the kernel were substituted with reduced graphene oxide, while a graphene envelope was applied to the graphene framework. The density of the graphene filaments produced amounted to 0.23 g cm^{-3}, which is 7 and 86 less than that of standard carbon fibers (> 1.7 g cm^{-3}) and Au-wire (about 20 g cm^{-3}), respectively. Fully graphene filaments possess a high conductivity and a high specific surface area due to interpenetrating porous graphene grids. Such materials consisting of graphene filaments with the use of a gel electrolyte H_2SO_4/PVA can be utilized as a basis of SCs having spring properties, high compressibility and extensibility, and a specific capacity of 1.2–1.7 mF cm^{-2} [75]. While the graphene filaments produced are light, very flexible, and conductive, their specific surface area is considerably lower than that for an individual fiber due to interaction between neighboring graphene sheets.

Recent studies have indicated that hybrid materials combining 2D graphene sheets with 1D CNTs possess a synergy effect, which manifests itself in a notable enhancement of electric and thermal conductivity and mechanical flexibility compared to the parameters of involved components. Cheng et al. [76] produced hybrid CNT/graphene filaments with a specific capacity of 1.2–1.3 mF cm^{-2} and preserving stable C – V characteristics even after 200 bending cycles in textile structures. However, such SCs are easily subject to short circuiting at contacts with each other. Kou et al. [75] have developed an assembly procedure of coaxial wet spinning for continuous production of graphene/CNT filaments wrapped into sodium carboxymethylcellulose (CMC) (Fig. 14). The CMC envelope effectively prevents the risk of a short circuit. The specific capacity reaches about 177 mF cm^{-2} due to a high specific surface area and effective inter-electrode ion transportation. The arrow in Fig. 14a shows the gel electrolyte PVA/H_3PO_4, while the inset to Fig. 14b presents a schematic image of an SC based on coaxial filaments.

Coaxial filaments were also utilized in the work of Kou et al. [75], where two separate woven yarns served as the anode and the cathode of a textile SC (Fig. 15). An unique coaxial isolated structure of filament electrodes with SAS coverage

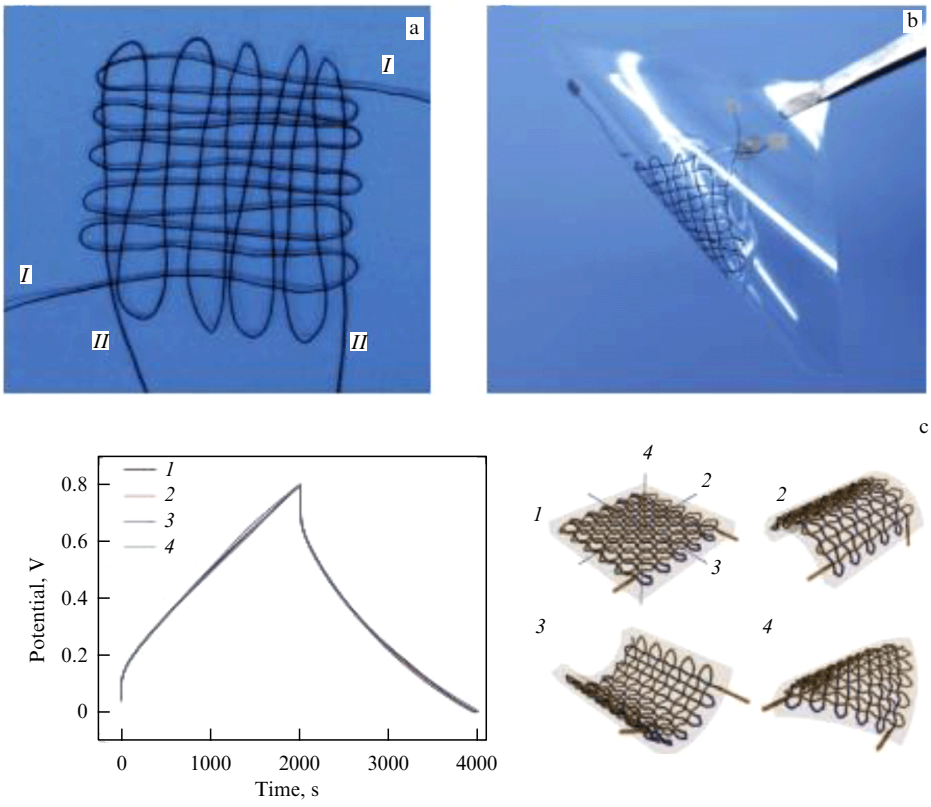

Figure 15. (a) Textile woven from two individual coaxial filaments. (b) Supercapacitor based on textile fabricated from two coaxial filaments. (c) GCD curves of filament SC (*1* — initial textile SC without bending, *2*, *3*, *4* — filament SC bent by 180° along three directions) [75].

Table 5. Characteristics of 1D graphene-based electrode materials utilized in SCs.

Electrode material	Method	Electrolyte	Test conditions	Capacity	Specific surface area	Literature
Flexible graphene filament	Direct electrochemical	H_2SO_4/PVA gel	30–500 mV s^{-1}	1.2–1.7 mF cm^{-2}	—	[74]
CNT/graphene filament	Thermal processing, CVD	1M Na_2SO_4	10–200 μA cm^{-2}	1.2–1.3 mF cm^{-2}	79.5 m^2 g^{-1}	[76]
Graphene/CNT filament wrapped with sodium carboxymethylcellulose	Wet spinning	PVA/H_3PO_4 gel	0.1 mA cm^{-2}	177 mF cm^{-2}	—	[75]
		1M H_2SO_4	0.1 mA cm^{-2}	269 mF cm^{-2}		
Reduced graphene oxide filament	Modified Hummers method, wet spinning	1M H_2SO_4	1 A g^{-1}	409 F g^{-1}	2210 m^2 g^{-1}	[79]
			100 A g^{-1}	56 F g^{-1}		
Cotton filaments, reduced graphene oxide/Ni	Electrochemical electrolysis, reduction in hydrazine vapor	1M Na_2SO_4	87.9 mA cm^{-3}	292.3 F cm^{-3}	—	[80]
Single walled CNTs, reduced graphene oxide doped with nitrogen	Hydrothermal, thermal processing	1M H_2SO_4	73.5 mA cm^{-3}	305 F cm^{-3}	396 m^2 g^{-1}	[81]
		PVA/H_3PO_4	26.7 mA cm^{-3}	300 F cm^{-3}		

permits avoiding a short circuit. The capacity of the textile SC amounts to 28 mF g^{-1} at a current of 10 mA g^{-1}, which exceeds the corresponding parameter of a commercial SC (25 mF g^{-1}) [77]. The corresponding GCD curves do not change at a bending angle of 180° along 3 directions (Fig. 15c), which demonstrates the superior flexibility of textile SCs woven from coaxial filaments.

A further increase in the specific energy is reached as a result of using asymmetric SCs based on graphene filaments. Wang et al. [78] prepared solid state SCs in which titanium wires covered with Co_3O_4 and a graphene filament were used as anode and cathode, respectively. The operating voltage can be increased to 1.5 V, the specific energy, to 0.62 mWh cm^{-3}, and the specific power, to 1.47 W cm^{-3}.

While filament SCs are of a great interest due to their high flexibility and weaving capacity, there are some problems requiring further effort to develop a device with high specific energy and power. Further work should focus on lowering unwanted disordering of graphene sheets and on modulating microporous structures inside graphene filaments in order to develop hierarchically structured nanocomposite electrodes.

Table 5 presents results of studying 1D graphene-based electrode materials in SCs, including the preparation method and the capacity values.

5.4.3 Graphene-based 2D electrode materials (2D graphene-based films). One 2D graphene film is graphene paper. The great interest in this material is due to its adjustable thickness, structural flexibility, light weight, and electrical properties, which is important for flexible SCs. As in the case of other graphene-based materials, processing thin graphene films and paper is hindered by the agglomeration and disordering of graphene sheets, resulting in a considerable decrease in the specific surface area and in limitations on electrolyte ion diffusion between graphene layers [86–88]. Numerous efforts, such as the addition of intermediate layers, template growth, and crumple of graphene sheets, have been mounted to overcome these factors [82–84].

An effective method of ordering graphene sheets relates to the use of suitable intermediate layers. Among the most widely studied intermediate layers, one should mention carbon-based materials (for example, carbon particles and CNTs), metals (for example, Pt and Au) or metal oxides (for example, SnO_2), and other pseudocapacitive materials (for example, transition metal oxides, hydroxides, and conducting polymers). Wang et al. [85] developed a flexible graphene paper containing a small quantity of technical carbon as an intermediate layer between graphene sheets. This creates an open structure for charge accumulation and channels for ion diffusion, which results in a considerable improvement in the electrochemical characteristics (specific capacity of 138 F g^{-1} in water electrolyte at a scanning rate of 10 mV s^{-1} and only a 3.85% decrease in capacity after 2000 cycles at a specific current of 10 A g^{-1}). Li et al. [86] reported on the development of a flexible graphene paper employing CNTs as an intermediate layer to prevent sheets from disordering. Hybrid electrodes with such a multi-layer structure possess a high specific capacity of 140 F g^{-1} at a specific current of 0.1 A g^{-1} in a 1-M solution of H_2SO_4. Si et al. [87] used Pt as an intermediate layer to separate graphene sheets and found a considerable increase in the specific capacity (269 F g^{-1}).

A further increase in the specific energy was reached through the use of pseudocapacitive materials with a high capacity: several transition metal oxides and hydroxides such as RuO_2, Fe_3O_4, CuO, $Ni(OH)_2$, MnO_2, Co_3O_4, and conducting polymers such as polyaniline (PANI), polypyrrole (PPy), and polythiophene (PT). Li et al. [88] developed a flexible film material for electrodes, where Li $Ni(OH)_2$ nanoplates were intercalated between tightly packed graphene sheets (Fig. 16a–c).

Furthermore, $Ni(OH)_2$ nanoplates placed between graphene sheets impart to them elasticity and an increased porosity (see inset in Fig. 16a). Figure 16d presents an image of the cross section of a film produced by means of ion beam treatment. The trench in the film was 5 μm in width and 6 μm in depth. A homogeneous distribution of the nanoplates between graphene layers is clearly visible in the image. An excellent distribution of the nanoplates $Ni(OH)_2$ between graphene sheets can also be seen in Fig. 16e and in the inset. The electrode produced provides a quite high specific capacity of 573 F g^{-1} at 0.2 A g^{-1}. A 250-fold increase in the specific current up to 50 A g^{-1} resulted in a decrease in the specific capacity of only 27.7%, to 413.5 F g^{-1}.

Graphene sheets intercalated with a conducting polymer are also of great interest. These composites are attractive especially for applications relating to energy storage, e.g., in SCs and batteries. The large specific surface energy of graphene combined with electrochemical properties of conducting polymers can result in the development of high-capacity and highly effective energy storage devices. Cheng

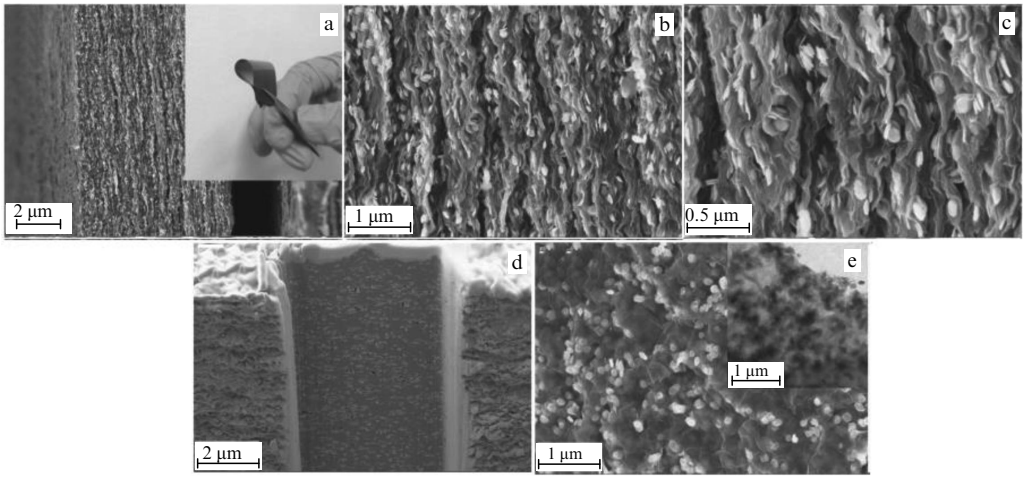

Figure 16. (a–c) Cross-sectional SEM images of dense graphene films intercalated with $Ni(OH)_2$ obtained at various amplifications; (d) side view of film treated by a focused ion beam (parallel to graphene sheets); (e) SEM and TEM (inset) images of film (perpendicular to graphene sheets) [88].

et al. [89] described the procedure for preparing a composite paper graphene-PANI using *in situ* anode polymerization of an aniline monomer on graphene paper. The hybrid film demonstrates a tensile strength of 12.6 MPa and specific capacity of 233 F g^{-1}, which exceeds by 58% that of graphene paper (147 F g^{-1}) and outperforms many other flexible carbon-based electrodes. This makes the hybrid film especially promising for flexible SCs.

Results of studying 2D graphene-based electrode materials for SCs, including the production method and capacity values, are presented in Table 6.

5.4.4 3D graphene-based electrode materials. Graphene-based nanocomposite films containing 2D graphene sheets with intermediate layers can be favorable in lowering the graphene aggregation which limits the access of ions to the common 2D structure. To further resolve this issue, significant efforts have been made to develop graphene-based macrostructures such as aerogels and graphene foams and sponges. These 3D graphene materials, possessing a high specific surface area and channels for rapid ion and electron transport, represent a very desirable field for the development of ways to enhance the specific energy and power and to improve the total SC productivity [63].

Chen et al. [93] utilized as hard templates monodispersed polymethylmethacrylate (PMMA) spheres, which were then deleted by annealing at 800 °C. The 3D structure produced in the form of bubbles provides managed and quite uniformly distributed micropores, which results in keeping a 67.9% capacity in the enhancement of the scanning rate up to 1000 mV s^{-1} (Fig. 17).

In addition to 3D graphene foams produced using polymer spheres as templates, chemical vapor deposition (CVD) on a Ni foam is also utilized as an effective process for the synthesis of graphene foams. Such structures can be seamless, unbroken, and highly conductive with a few defects, which makes them a suitable material for the production of monolithic 3D nanocomposite electrodes. Cao et al. [94] prepared 3D graphene networks using as a template Ni foam and a simple CVD process with ethanol as the carbon source (Fig. 18). The 3D graphene networks produced have proven to be excellent templates for producing composite

Table 6. Characteristics of 2D graphene-based electrode materials in SCs.

Electrode material	SAS	Electrolyte	Testing conditions	Specific capacity	Specific surface area	Literature
Flexible graphene paper with addition of technical carbon	Vacuum filtration	6M KOH	10 mV s^{-1}	138 F g^{-1}	—	[85]
CNT/graphene oxide	Vacuum filtration	1M H_2SO_4	0.1 A g^{-1}	140 F g^{-1}	—	[86]
Pt/graphene	Chemical reduction	0.5M H_2SO_4	50 mV s^{-1}	269 F g^{-1}	862 m^2 g^{-1}	[87]
Graphene/$Ni(OH)_2$ film	Filtration with self-assembly	1M KOH	0.2 A g^{-1}	573 F g^{-1}	—	[88]
			50 A g^{-1}	413.5 F g^{-1}		
Graphene/PANI paper	*In situ* anode electro-chemical polymerization	1M H_2SO_4	2 mV s^{-1}	233 F g^{-1}	39 m^2 g^{-1}	[89]
Graphene/PANI	Polymerization	1M H_2SO_4	0.5 A g^{-1}	385 F g^{-1}	116.2 m^2 g^{-1}	[90]
			1 A g^{-1}	362 F g^{-1}		
Graphene nanosheets/PANI	*In situ* polymerization	6M KOH	1 mV s^{-1}	1046 F g^{-1}	—	[91]
PEDOT/reduced graphene oxide	Electro-polymerization, electro-chemical reduction	$BMIMBF_4$	50 mV s^{-1}	14 F cm^{-2}	—	[92]

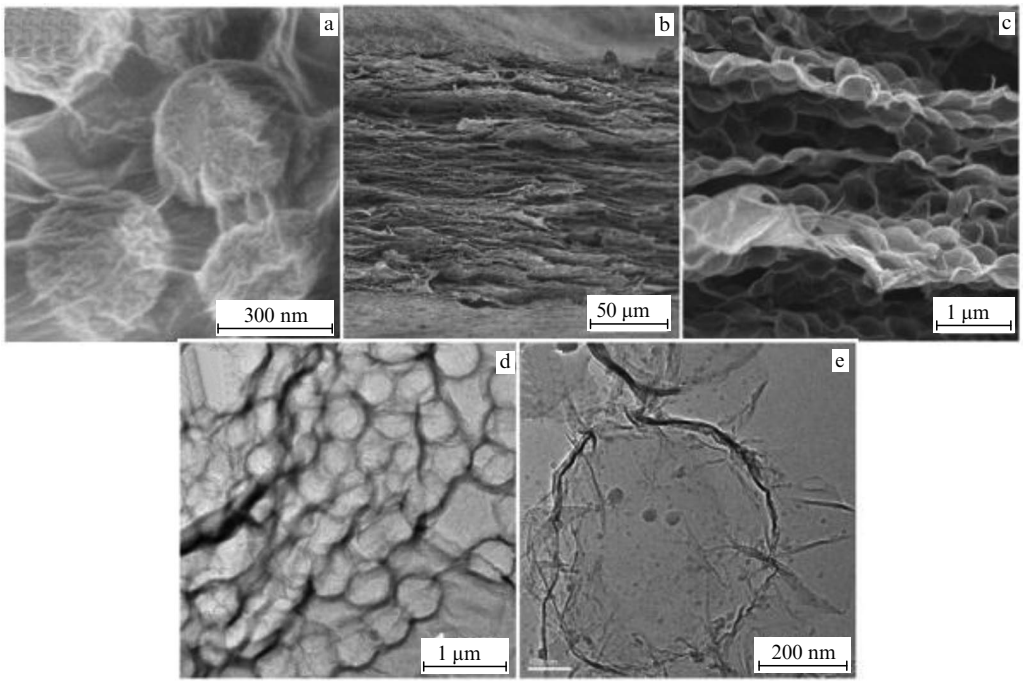

Figure 17. SEM images of surface (a) and cross section of graphene-PMMA film with low (b) and high (c) amplification; TEM images of graphene bubbles inside graphene-PMMA film sample with low (d) and high (e) resolution [93].

graphene/metal oxide for SC application. Nickel oxide (NiO) was deposited electrochemically onto 3D graphene networks for the production of 3D graphene/NiO nanocomposites for SC electrodes. These nanocomposites possess an electric conductivity close to that of pure graphene and a high specific surface area, which promotes rapid access of electrolyte ions to the NiO surface and facilitates rapid electron transport between active materials and the current collector in an SC. The 3D graphene/NiO nanocomposite possesses a high specific capacity of 816 F g^{-1} at a scanning rate of 5 mV s^{-1} and a stable cycling productivity without a notable decrease after 2000 cycles.

Graphene hydrogels and aerogels are a new class of ultralight porous materials possessing a high ratio of strength to mass and a high ratio of specific surface area to volume. Hydrogels (also known as hydrophilic gels) are polymers adsorbing a large quantity of water without dissolution. The capability of hydrogels to conduct water sorption is due to the existence of hydrophilic functional groups attached to the basic polymer chain, while their dissolution resistance is because of cross linking between network chains. Water existing inside a hydrogel provides free diffusion of some dissolved molecules, while a polymer plays the role of the matrix keeping the water. Hydrogels are characterized by a good osmotic capacity, a high water sorption capability, and good elasticity. Along with wide use in everyday life (for example, fruit jelly, contact lenses, hair gel), they are also utilized in energy storage devices (for example, SCs). In such systems, a hydrogel is mixed with electric conducting additives such as graphene, which results in the formation of a conducting composite. The aerogel structure is similar to that of hydrogels. An aerogel can be synthesized by substituting the liquid in a hydrogel or other wet gel with air without destroying the interconnected microstructure. Aerogels are characterized by a low density (0.004–0.500 g cm^{-3}) [95] and a high porosity, which makes

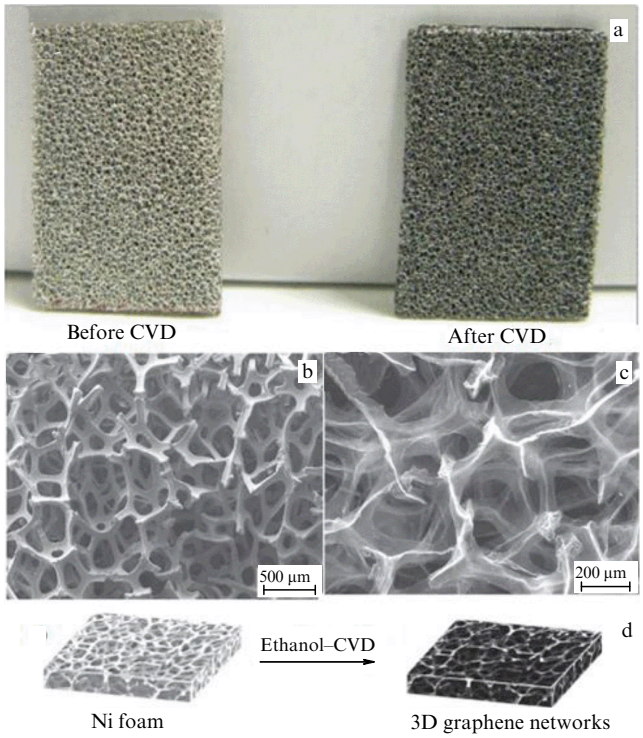

Figure 18. (a) Photos of Ni foam before and after graphene growth. (b) SEM images of 3D graphene networks grown on Ni foam after CVD. (c) 3D graphene network after removal of Ni foam. (d) Schematic illustration of synthesis of 3D graphene network on Ni foam by CVD method using ethanol [94].

them a suitable material for many applications, such as SCs, adsorbents, and Li-ion batteries.

In recent years, graphene-based hydrogels and aerogels have become the subject of intensive research in terms of their

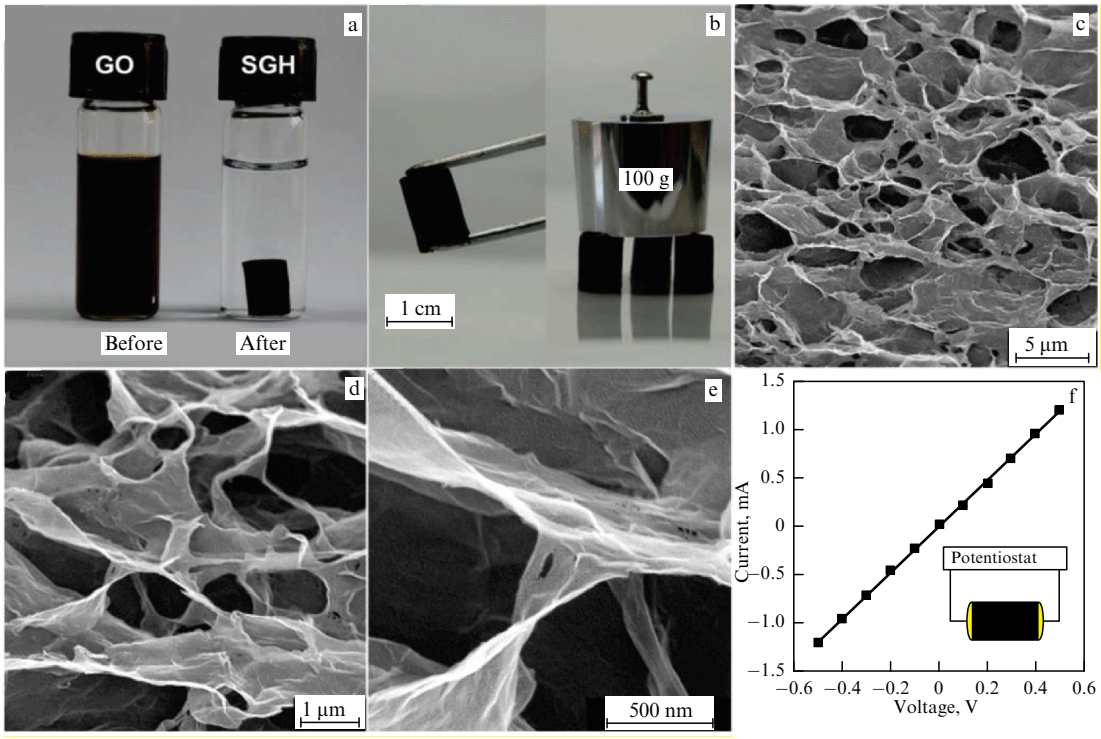

Figure 19. (a) Photo of a homogeneous water graphene oxide dispersion with a concentration of 2 mg ml^{-1} before and after hydrothermal reduction at 180 °C for 12 h. (b) Photo of rigid self-assembling graphene hydrogel providing ease of use and retaining mass. (c–e) SEM images of inner microstructure of self-assembling graphene hydrogel at different amplifications. (f) Current-voltage characteristic of the self-assembled graphene hydrogel at a room temperature; the inset presents the two-probe method for measuring the conductivity [96].

usage in SCs. Usually, graphene-based hydrogels are produced by using graphene oxide as building blocks. There are several methods of formation of graphene oxide gels, including self assembly through a hydrothermal reaction, formation induced by ions or polymers, and chemical bond tailoring. Xu et al. [96] have described graphene hydrogels produced through the hydrothermal processing of a graphene oxide suspension (Fig. 19). The graphene hydrogels produced demonstrate good mechanical properties, excellent electric conduction, and a high specific capacity on the level of 175 F g^{-1}.

Recently, Yang et al. [97] prepared a graphene hydrogel film tightly packed using the capillary compression method. They confirmed the advantages of flexible graphene hydrogel films possessing a low resistance to ion transport and a high surface accessible for ions, which result in excellent SC characteristics (255.5 F cm^{-3} in water electrolytes and 261.3 F cm^{-3} in organic electrolytes at the specific current of 0.1 A g^{-1}). A high productivity of tightly packed graphene hydrogel films has great potential for large-scale real applications, because the production methods are conceptually compatible with the traditional paper production process and can be easily scaled. The porous structure of graphene hydrogels can permit the insertion of other nanomaterials into 3D networks in order to form graphene hydrogel-based composite materials. One can expect that a further improvement in the characteristics of SCs will be reached by combining graphene hydrogels with other materials such as conducting polymers, metal oxides, and CNTs due to a synergy effect. Zhou et al. [98] have prepared a hybrid hydrogel containing graphene and poly(3,4-ethylenedioxythiophene) (PEDOT). This hybrid hydrogel demonstrates excellent mechanical characteristics, a high specific capacity of 174.4 F g^{-1}, and good electric conductivity (0.73 S cm^{-1}). These superior properties may be due to a synergistic combination of the high properties of graphene and pseudocapacity of PEDOT. Composite graphene/$Ni(OH)_2$ hydrogels were prepared and successfully used 3D electrode materials for SCs [99]. These hybrid hydrogels have demonstrated a high specific capacity of 1247 F g^{-1} at a voltage scanning rate of 5 mV s^{-1} and a superior cycling stability. Composite electrode materials exhibit a high capacity efficiency, which may be effected by a synergistic effect of high conductivity and electrochemical stability of graphene hydrogels, as well as a short charge transport distance between graphene hydrogel and a current collector. Table 7 contains the results of a study of graphene hydrogel-based SCs, including the production method and the capacity values.

The substitution of the filling medium (water) in graphene hydrogels with air without destroying the network structure can result in another 3D network, graphene aerogels. As a rule, graphene aerogels are prepared through supercritical or sublimation drying of wet graphene-based gels. Graphene aerogels have been actively under study in recent years, because they represent large 3D networks with a ceaseless porous structure and a large surface area. This unique structure can provide effective ion transport and adsorption, which results in a high productivity of SCs. In recent years, reduced graphene oxide aerogels have been successfully produced and studied as electrode materials for SCs. Liu et al. [116] fabricated a flexible folded graphene paper from thermally reduced graphene oxide aerogels. Notably, oxide graphene aerogel was prepared by sublimation drying of a

Table 7. Characteristics of graphene gel-based SCs.

Production method	Modification	Specific surface area and pore size	Specific capacity	Testing conditions	Electrolyte	Literature
Hydrothermal	—	—, —	175 F g^{-1}	1 A g^{-1}, two electrodes	5M KOH	[96]
Chemical reaction	Ethylene-diamine	745 m^2 g^{-1}, 47 nm	232 F g^{-1}	1 A g^{-1}, two electrodes	2M KOH	[100]
Hydrothermal	Organic amine	—, —	190.1 F g^{-1}	10 A g^{-1}, two electrodes	5M KOH	[101]
Hydrothermal	Urea	> 1300 m^2 g^{-1}, 1.7–4.3 nm	308 F g^{-1}	3 A g^{-1}, three electrodes	6M KOH	[102]
Hydrothermal	Hydroxylamine	—, —	205 F g^{-1}	1 mV s^{-1}, two electrodes	25% KOH	[103]
Hydrothermal	—	414 m^2 g^{-1}, 2–70 nm	186 F g^{-1}	1 A g^{-1}, two electrodes	H_2SO_4-PVA gel	[104]
Hydrothermal	—	951 m^2 g^{-1}, —	220 F g^{-1}	1 A g^{-1}, two electrodes	5M KOH	[105]
Chemical reduction	L-glutathione	315.2 m^2 g^{-1}, 2–10 nm	157.7 F g^{-1}	1 A g^{-1}, two electrodes	0.5M Na_2SO_4	[106]
Chemical reduction	Sodium ascorbate	—, —	240 F g^{-1}	1.2 A g^{-1}, three electrodes	1M H_2SO_4	[107]
Filtration	—	—, —	255.5 F cm^{-3}	0.1 A g^{-1}, two electrodes	1M H_2SO_4	[108]
			261.3 F cm^{-3}	0.1 A g^{-1}, two electrodes	$EMIMBF_4$/AN	
Chemical reduction	PANI	—, —	334 F g^{-1}	2 A g^{-1}, three electrodes	6M KOH	[109]
Cross-linking of polymers	PEDOT	—, —	104 F g^{-1}	0.5 A g^{-1}, two electrodes	1M Na_2SO_4	[110]
Hydrothermal	PPy	463 m^2 g^{-1}, —	330 F g^{-1}	1.5 A g^{-1}, three electrodes	3M $NaClO_4$	[111]
Hydrothermal	Co_3O_4	—, —	757.5 F g^{-1}	0.5 A g^{-1}, three electrodes	6M KOH	[112]
Hydrothermal	CNTs	237 m^2 g^{-1}, —	318 F g^{-1}	0.1 A g^{-1}, two electrodes	30% KOH	[113]
Hydrothermal	Hydroquinones	297 m^2 g^{-1}, 2–70 nm	441 F g^{-1}	1 A g^{-1}, two electrodes	1M H_2SO_4	[114]
Hydrothermal	$Ni(OH)_2$	92 m^2 g^{-1}, —	1247 F g^{-1}	5 mV s^{-1}, three electrodes	6M KOH	[99]
Deposition	Nickel foam	1260–1725 m^2 g^{-1}, —	45.6 mF cm^{-2}	0.67 mA cm^{-2}, two electrodes	5M KOH	[115]

homogeneous water oxide graphene dispersion (5 mg ml^{-1}) in a Petri dish. Then, graphene oxide aerogel was transformed into graphene aerogel by means of direct heating in a preheated electrical furnace in the air at 200 °C for 1.5 h. Graphene paper about 10 μm in depth was produced by extrusion of graphene aerogel at 10 MPa. The authors of [116] have demonstrated that graphene paper-based electrodes exhibit better capacitance characteristics than available carbon materials do. Moreover, these types of electrodes are more flexible, do not contain binders, and are suitable for mass production. Many researchers are focused on producing graphene aerogel-based composite materials for SCs. Wu et al. [117] synthesized graphene aerogels doped with nitrogen and boron, inserting ammoniacal boron trifluoride into wet gels with step-by-step sublimation drying. They produced an entirely solid-state SC using doped graphene aerogels as electrode materials and PVA–H_2SO_4 gel as the electrolyte. Entirely solid-state SCs have exhibited a specific capacity of about 62 F g^{-1}, specific power of about 1600 W kg^{-1}, and excellent cycling stability. Metal oxides are also inserted into graphene aerogel networks to form composite materials. Wu et al. [118] prepared graphene-based composite aerogels by doping with metal oxides such as Co_3O_4 and RuO_2. Graphene aerogels loaded with metal oxides exhibit a superior specific capacity of 226 F g^{-1}, a high charging/discharging rate, and an excellent cycling capacity due to a combination of effects of metal oxide pseudocapacity, large surface area, high conductivity, and electrochemical stability. Table 8 presents results of studies of graphene aerogel-based SCs, including synthesis methods and capacity values.

It is obvious that the important characteristics of SCs such as the specific capacity, specific energy, and service life have undergone significant changes since the graphene's appearance. SCs feature a high specific power (up to 10,000 W kg^{-1} [5]), which allows them to very quickly charge and discharge; however, the specific capacity and the specific energy of SCs

Table 8. Characteristics of graphene aerogel-based SCs.

Production method	Modification	Specific surface area and pore size	Specific capacity, F g^{-1}	Testing conditions	Electrolyte	Literature
Lyophilization	—	—, —	172	1 A g^{-1}, two electrodes	1M H_2SO_4	[116]
Supercritical drying	—	870 m^2 g^{-1}, 2–50 nm	153	0.1 A g^{-1}, three electrodes	Ion liquid	[119]
Lyophilization	L-Ascorbic acid	512 m^2 g^{-1}, 1.5–55 nm	128	0.05 A g^{-1}, two electrodes	6M KOH	[120]
Supercritical drying	Hypophosphorous acid	830 m^2 g^{-1}, 4 nm	278.6	0.2 A g^{-1}, three electrodes	1M H_2SO_4	[121]
Lyophilization	Nitrogen and boron doping	249 m^2 g^{-1}, —	62	5 mV s^{-1}, three electrodes	H_2SO_4-PVA	[122]
Lyophilization	Glucose	12.5–364.6 m^2 g^{-1}, —	161.6	0.5 A g^{-1}, three electrodes	Na_2SO_4	[123]
Lyophilization	Metal oxides	350 m^2 g^{-1}, 2–3.5 nm	226	1 mV s^{-1}, three electrodes	1M H_2SO_4	[118]
Pyrolysis	Carbon	361–763 m^2 g^{-1}, 10–50 nm	122	0.05 A g^{-1}, two electrodes	6M KOH	[124]

with traditional electrode materials such as porous carbon are rather low (120–200 F g^{-1} [125] and 1–10 Wh kg^{-1} [5], respectively). This limits the potential to use them in devices requiring long-term energy storage. Graphene with a very large specific surface area (up to 2630 m^2 g^{-1} [41]) permits enhancing the specific capacity of SCs to 200–500 F g^{-1} [126] or even more in some cases. It is due mainly to a larger area for storing the charge on the electrode surface. The appearance of graphene also promotes an increase in the specific energy of SCs up to 60–136 Wh kg^{-1} [127]. While it still does not reach the level of Li-ion batteries, the specific energy of SCs has been enhanced considerably, which expands their use, especially in electric transport and electronic devices. Graphene also promotes an enhancement of the service life of SCs due to high chemical and mechanical stability. Studies [125] have indicated that after 10,000 cycles graphene-based SCs maintain 96% of their initial capacity.

Graphene brought many significant improvements to SCs, making them more effective and durable and offering new prospects for their application in the field of energy storage.

6. Conclusions

One effective approach to solving problems of storage and subsequent usage of electric energy relates to the development and improvement of SCs. These devices are considered as an alternative to traditionally utilized Li-ion batteries in connection with the projected depletion of reserves of Li in Earth's crust and the rather limited operational characteristics of those batteries. The scope of use of SCs as electric energy accumulators is continuously expanding. Along with this, the efforts of many laboratories are focused on improving the operational characteristics of these devices, such as specific energy stored, specific released power, charge/discharge time, and the ability to withstand a maximum quantity of charge/discharge cycles without lowering the stored energy level. Progress in developing SCs relates first to the use of new electrode materials. Therewith, graphene-based materials successfully combining such properties as miniature size, good electric conduction, and high chemical and mechanical stability are attracting considerable attention Many tens of studies are devoted to the investigation of graphene-based materials in terms of their utilization as electrodes in SCs. Studies performed have shown that such materials possess a considerable potential in terms of the enhancement of operational characteristics of SCs. Obstacles along the way relate to the rather high production cost of graphene and graphene-based materials and to the necessity of implementing such production in the existing microelectronics industry. One can expect that the obstacles noted will be overcome in the coming years and SCs with graphene-based electrodes will take their rightful place in modern technology.

The work was carried out within the framework of State Tasks FSWF-2023-0016 and FSWF-2025-0001.

References

1. Idumah C I *Polymer-Plastics Technol. Mater.* **61** 1871 (2022)
2. Allen M J, Tung V C, Kaner R B *Chem. Rev.* **110** 132 (2010)
3. Volfkovich Yu M *Russ. J. Electrochem.* **57** 311 (2021); *Elektrokhimiya* **57** (4) 197 (2021)
4. Kötz R, Carlen M *Electrochim. Acta* **45** 2483 (2000)
5. Thota S P et al. *Engineered Science* **18** 31 (2022) https://doi.org/10.30919/es8d664
6. Raza W et al. *Nano Energy* **52** 441 (2018)
7. Horn M et al. *Economic Anal. Policy* **61** 93 (2019)
8. Wang G, Zhang L, Zhang J *Chem. Soc. Rev.* **41** 797 (2012)
9. Zheng J P, Huang J, Jow T R *J. Electrochem. Soc.* **144** 2026 (1997)
10. Burke A *J. Power Sources* **91** 37 (2000)
11. Burke A F *Proc. IEEE* **95** 806 (2007)
12. Sarno M, in *Catalysis, Green Chemistry and Sustainable Energy* (Studies in Surface Science and Catalysis, Vol. 179, Eds A Basile et al.) (Amsterdam: Elsevier, 2019) p. 431, https://doi.org/10.1016/B978-0-444-64337-7.00022-7
13. Conway B E *Electrochemical Supercapacitors*: *Scientific Fundamentals and Technological Applications* (New York: Kluwer Acad./Plenum Publ., 1999) https://doi.org/10.1007/978-1-4757-3058-6
14. Herrero E, Buller L J, Abruña H D *Chem. Rev.* **101** 1897 (2001)
15. Helmholtz H *Ann. Physik* **243** 337 (1879)
16. Chapman D L *Philos. Mag.* **25** 475 (1913)
17. Stern O *Z. Elektrochem. angew. phys. Chem.* **30** 508 (1924) https://doi.org/10.1002/bbpc.192400182
18. Zhang L L, Zhao X S *Chem. Soc. Rev.* **38** 2520 (2009)

19. Becker H I "Low voltage electrolytic capacitor", U.S. Patent No. 2800616 (1957); https://patents.google.com/patent/US2800616A/en
20. Rightmire R A "Electrical energy storage apparatus", U.S. Patent No. 3288641 (1962); https://patents.google.com/patent/US3288641A/en
21. Boos D L "Electrolytic capacitor having carbon paste electrodes", U.S. Patent No. 3536963 (1970); https://patents.google.com/patent/US3536963A/en
22. Li X, Wei B *Nano Energy* **2** (2) 159 (2013)
23. Zil'berman G E *Elektrichestvo i Magnetizm* (Electricity and Magnetism) (Dolgoprudnyi: Intellekt, 2015)
24. Miller J R, Dimon P *Science* **321** 651 (2008)
25. Brett C M A, Brett A M O *Electrochemistry*: *Principles, Methods, and Applications* (Oxford: Oxford Univ. Press, 1993)
26. Pal B et al. *Nanoscale Adv*. **1** 3807 (2019)
27. Choudhury N A, Sampath S, Shukla A K *Energy Environ. Sci*. **2** 55 (2009)
28. Sequeira C, Santos D (Eds) *Polymer Electrolytes*: *Fundamentals and Applications* (Cambridge: Woodhead Publ., 2010)
29. Zhong C et al. *Chem. Soc. Rev*. **44** 7484 (2015)
30. Armand M et al. *Nature Mater*. **8** 621 (2009)
31. Hall P J et al. *Energy Environ. Sci*. **3** 1238 (2010)
32. Pandolfo A G, Hollenkamp A F *J. Power Sources* **157** 11 (2006)
33. Sun Y, Wu Q, Shi G *Energy Environ. Sci*. **4** 1113 (2011)
34. Dubey R, Guruviah V *Ionics* **25** 1419 (2019)
35. Borenstein A et al. *J. Mater. Chem. A* **5** 12653 (2017)
36. Sing K S W et al. *Pure Appl. Chem*. **57** 603 (1985)
37. Zhu H et al. (Eds) *Graphene*: *Fabrication, Characterizations, Properties and Applications* (London: Academic Press, 2017)
38. Dubois S M-M et al. *Eur. Phys. J. B* **72** 1 (2009)
39. Geim A K, Novoselov K S *Nature Mater*. **6** 183 (2007)
40. Lee T-W *Graphene for Flexible Lighting and Displays* (Cambridge, MA: Woodhead Publ., 2020)
41. Stoller M D et al. *Nano Lett*. **8** 3498 (2008)
42. Kelly B T *Physics of Graphite* (London: Applied Science, 1981)
43. Morozov S V et al. *Phys. Rev. Lett*. **100** 016602 (2008)
44. Boscá A et al. *J. Appl. Phys*. **117** 044504 (2015)
45. Si C, Sun Z, Liu F *Nanoscale* **8** 3207 (2016)
46. Nair R R et al. *Science* **320** 1308 (2008)
47. Berger C et al. *Science* **312** 1191 (2006)
48. Patel R B et al. *J. Mater. Res*. **29** 1522 (2014)
49. Pei S, Cheng H-M *Carbon* **50** 3210 (2012)
50. Larciprete R et al. *J. Am. Chem. Soc*. **133** 17315 (2011)
51. Dreyer D R et al. *Chem. Soc. Rev*. **39** 228 (2010)
52. Bocharov G S, Eletskii A V *J. Struct. Chem*. **59** 806 (2018); *Zh. Strukt. Khim*. **59** 841 (2018)
53. McAllister M J et al. *Chem. Mater*. **19** 4396 (2007)
54. Agarwal V, Zetterlund P B *Chem. Eng. J*. **405** 127018 (2021)
55. Schniepp H C et al. *J. Phys. Chem. B* **110** 8535 (2006)
56. Becerril H A et al. *ACS Nano* **2** 463 (2008)
57. Wang X, Zhi L, Müllen K *Nano Lett*. **8** 323 (2008)
58. Wu Z-S et al. *Carbon* **47** 493 (2009)
59. Wu Z-S et al. *ACS Nano* **3** 411 (2009)
60. Li X et al. *J. Am. Chem. Soc*. **131** 15939 (2009)
61. Bocharov G S, Eletskii A V, Melnikov V P *Nanosyst. Phys. Chem. Math*. **9** (1) 98 (2018)
62. Sharon M, Sharon M (Eds) *Graphene*: *An Introduction to the Fundamentals and Industrial Applications* (Hoboken, NJ: Wiley, 2015)
63. Ke Q, Wang J *J. Materiomics* **2** 37 (2016)
64. Zhang K et al. *J. Mater. Chem*. **21** 7302 (2011)
65. Mao L et al. *J. Mater. Chem*. **22** 80 (2012)
66. Li Z et al. *J. Power Sources* **196** 8160 (2011)
67. Wang H et al. *J. Am. Chem. Soc*. **132** 7472 (2010)
68. Wang H-W et al. *Mater. Chem. Phys*. **130** 672 (2011)
69. Yoon S-M et al. *ACS Nano* **6** 6803 (2012)
70. Lee J-S et al. *ACS Nano* **7** 6047 (2013)
71. Park S-H et al. *Chem. Mater*. **27** 457 (2015)
72. Ke Q et al. *Mater. Res. Express* **1** 025015 (2014)
73. Ke Q et al. *RSC Adv*. **4** 26398 (2014)
74. Meng Y et al. *Adv. Mater*. **25** 2326 (2013)
75. Kou L et al. *Nat. Commun*. **5** 3754 (2014)
76. Cheng H et al. *Nanoscale* **5** 3428 (2013)
77. Pech D et al. *Nature Nanotechnol*. **5** 651 (2010)
78. Wang X et al. *Angew. Chem. Int. Ed*. **53** 1849 (2014)
79. Aboutalebi S H et al. *ACS Nano* **8** 2456 (2014)
80. Liu L et al. *Nat. Commun*. **6** 7260 (2015)
81. Yu D et al. *Nature Nanotechnol*. **9** 555 (2014)
82. Lei Z, Christov N, Zhao X S *Energy Environ. Sci*. **4** 1866 (2011)
83. Vickery J L, Patil A J, Mann S *Adv. Mater*. **21** 2180 (2009)
84. Khan A A et al. *J. Phys. Chem. B* **128** 9586 (2024)
85. Wang G et al. *Small* **8** 452 (2012)
86. Qiu L et al. *Chem. Eur. J*. **16** 10653 (2010)
87. Si Y, Samulski E T *Chem. Mater*. **20** 6792 (2008)
88. Li M et al. *Adv. Funct. Mater*. **24** 7495 (2014)
89. Wang D-W et al. *ACS Nano* **3** 1745 (2009)
90. Meng Y et al. *Adv. Mater*. **25** 6985 (2013)
91. Yan J et al. *Carbon* **48** 487 (2010)
92. Lehtimäki S et al. *ACS Appl. Mater. Interfaces* **7** 22137 (2015)
93. Chen C-M et al. *Chem. Commun*. **48** 7149 (2012)
94. Cao X et al. *Small* **7** 3163 (2011)
95. Muhammad A et al. *Polymers* **13** 1347 (2021)
96. Xu Y et al. *ACS Nano* **4** 4324 (2010)
97. Yang T et al. *J. Mater. Chem. A* **5** 16537 (2017)
98. Zhou H et al. *Carbon* **59** 495 (2013)
99. Xu Y et al. *Nano Res*. **6** 65 (2013)
100. Luan V H et al. *J. Mater. Chem. A* **1** 208 (2013)
101. Chen P et al. *Nano Energy* **2** 249 (2013)
102. Guo H-L et al. *J. Mater. Chem. A* **1** 2248 (2013)
103. Chang Y et al. *J. Power Sources* **238** 492 (2013)
104. Xu Y et al. *ACS Nano* **7** 4042 (2013)
105. Zhang L, Shi G *J. Phys. Chem. C* **115** 17206 (2011)
106. Gao H et al. *ACS Appl. Mater. Interfaces* **4** 2801 (2012)
107. Sheng K et al. *New Carbon Mater*. **26** 9 (2011)
108. Yang X et al. *Science* **341** 534 (2013)
109. Tai Z, Yan X, Xue Q *J. Electrochem. Soc*. **159** A1702 (2012)
110. Zhang X et al. *J. Mater. Chem*. **21** 6494 (2011)
111. Zhao Y et al. *Adv. Mater*. **25** 591 (2013)
112. Yuan J et al. *Phys. Chem. Chem. Phys*. **15** 12940 (2013)
113. Wang Y et al. *J. Phys. Chem. C* **115** 23192 (2011)
114. Xu Y et al. *Adv. Mater*. **25** 5779 (2013)
115. Chen J et al. *Adv. Mater*. **24** 4569 (2012)
116. Liu F et al. *Adv. Mater*. **24** 1089 (2012)
117. Wu X-L, Xu A-W *J. Mater. Chem. A* **2** 4852 (2014)
118. Wu Z-S et al. *J. Am. Chem. Soc*. **134** 19532 (2012)
119. Wu X et al. *J. Mater. Chem*. **22** 23186 (2012)
120. Zhang X et al. *J. Mater. Chem*. **21** 6494 (2011)
121. Si W et al. *Nanoscale Res. Lett*. **8** 247 (2013)
122. Wu Z-S et al. *Adv. Mater*. **24** 5130 (2012)
123. Ji C-C et al. *J. Colloid Interface Sci*. **407** 416 (2013)
124. Meng F et al. *J. Mater. Chem*. **21** 18537 (2011)
125. Bokhari S W et al. *Energy Rep*. **6** 2768 (2020)
126. Kumar N et al. *Nanomaterials* **12** 3708 (2022)
127. Liu C et al. *Nano Lett*. **10** 4863 (2010)
128. Novoselov K S et al. *Science* **306** 666 (2004)
129. Eletskii A V et al. *Phys. Usp*. **58** 209 (2015); *Usp. Fiz. Nauk* **185** 225 (2015)